








Intrinsic GATA4 expression sensitizes the aortic root to dilation in a Loeys–Dietz syndrome mouse model

Received: 14 May 2024

Accepted: 9 October 2024

Published online: 20 November 2024

 Check for updates

Emily E. Bramel ^{1,2}, Wendy A. Espinoza Camejo^{1,2}, Tyler J. Creamer^{1,3}, Leda Restrepo ¹, Muzna Saqib¹, Rustam Bagirzadeh¹, Anthony Zeng ¹, Jacob T. Mitchell ^{1,2}, Genevieve L. Stein-O'Brien^{1,4}, Albert J. Pedroza ⁵, Michael P. Fischbein⁵, Harry C. Dietz ¹ & Elena Gallo MacFarlane ^{1,3} ✉

Loeys–Dietz syndrome (LDS) is a connective tissue disorder caused by mutations that decrease transforming growth factor- β signaling. LDS-causing mutations increase the risk of aneurysm throughout the arterial tree, yet the aortic root is a site of heightened susceptibility. Here we investigate the heterogeneity of vascular smooth muscle cells (VSMCs) in the aorta of *Tgfr1*^{M318R/+} LDS mice by single-cell transcriptomics to identify molecular determinants of this vulnerability. Reduced expression of components of the extracellular matrix–receptor apparatus and upregulation of stress and inflammatory pathways were observed in all LDS VSMCs. However, regardless of genotype, a subset of *Gata4*-expressing VSMCs predominantly located in the aortic root intrinsically displayed a less differentiated, proinflammatory profile. A similar population was also identified among aortic VSMCs in a human single-cell RNA sequencing dataset. Postnatal VSMC-specific *Gata4* deletion reduced aortic root dilation in LDS mice, suggesting that this factor sensitizes the aortic root to the effects of impaired transforming growth factor- β signaling.

Thoracic aortic aneurysms are localized vascular dilations that increase the risk of fatal dissections and/or rupture of the vessel wall¹. Effective medical therapies to prevent life-threatening aortic events remain elusive¹. Loeys–Dietz syndrome (LDS) is a hereditary connective tissue disorder that presents with highly penetrant aortic aneurysms². LDS is caused by heterozygous, loss-of-function mutations in genes coding for positive effectors of the transforming growth factor- β (TGF- β) signaling pathway, including receptors, ligands and intracellular signaling mediators^{3–7}. All of these mutations result in reduced phosphorylation/activation of Smad2 and Smad3, leading to defective Smad-dependent transcriptional regulation. Secondary compensatory

mechanisms, including upregulation of angiotensin II type I receptor (AT1R) signaling and increased expression of TGF- β ligands and Smad proteins, ultimately elevate levels of Smad2/Smad3 activity at diseased aortic sites, with outcomes ranging from adaptive to maladaptive, depending on the disease progression and cellular context^{3,5,6,8–10}. While LDS-causing mutations heighten aneurysm risk in all arteries, the aortic root is especially vulnerable to disease^{11–13}. Several laboratories have highlighted how the cellular composition and/or the mechanical stresses may contribute to the increased risk of disease in this location; however, the molecular determinants of this susceptibility remain unclear^{10,14,15}. Vascular smooth muscle cells (VSMCs) are the primary

¹McKusick-Nathans Department of Genetic Medicine, Johns Hopkins University School of Medicine, Baltimore, MD, USA. ²Predoctoral Training in Human Genetics and Genomics, Johns Hopkins University School of Medicine, Baltimore, MD, USA. ³Department of Surgery, Johns Hopkins University School of Medicine, Baltimore, MD, USA. ⁴Solomon H. Snyder Department of Neuroscience, Johns Hopkins University School of Medicine, Baltimore, MD, USA. ⁵Department of Cardiothoracic Surgery, Stanford University School of Medicine, Stanford, CA, USA. ✉e-mail: egallo1@jhmi.edu

cellular component of the aortic wall, but the heterogeneity of VSMCs within the aorta and its implications for aneurysm are not fully understood. In this study, we investigate the transcriptional heterogeneity of VSMCs in the normal and diseased murine aorta leveraging both single-cell RNA sequencing (scRNA-seq) and spatial analysis via high throughput in situ hybridization. We identify *Gata4* as a regional factor whose expression is intrinsically elevated in the aortic root and further upregulated in LDS samples. We also show that postnatal deletion of *Gata4* in VSMCs ameliorates aortic root dilation in a murine model of LDS harboring a *Tgfb1*^{M318R/+} genotype.

Results

Perturbed transcriptional profiles in *Tgfb1*^{M318R/+} VSMCs

LDS mouse models expressing a heterozygous missense mutation in *Tgfb1* (*Tgfb1*^{M318R/+}) develop highly penetrant aortic root dilation^{9,10}. To assess transcriptomic changes associated with vascular pathology in this model, we performed scRNA-seq on the aortic root and ascending aorta of control (*Tgfb1*^{+/+}) and LDS mice at 16 weeks of age, a time when dilation is consistently observed but before a decrease in survival below 90% (refs. 9,10).

This analysis resulted in the identification of all the expected cell types according to well-established expression profiles¹⁶ (Fig. 1a,b and Extended Data Fig. 1). In consideration of the critical role of VSMCs in the pathogenesis of aortic aneurysm¹⁷, we focused the downstream analysis of LDS-driven transcriptional alterations on this cell type (Supplementary Table 1). Using the Cytoscape¹⁸ ClueGO¹⁹ plug-in to leverage gene set enrichment information from multiple databases, we produced a network of functionally related terms and pathways that are differentially enriched among downregulated and upregulated transcripts (Fig. 1c,d and Supplementary Table 2). The *Tgfb1*^{M318R/+} LDS mutation caused broad downregulation of transcripts related to the maintenance of extracellular matrix (ECM)–receptor interactions and integrity of the elastic and contractile function of the aortic wall (Fig. 1c–e and Supplementary Table 2). Concurrently, the pathways involved in stress responses (that is, hypoxia and p53-dependent pathways), inflammation, senescence and cell death were enriched among transcripts upregulated in *Tgfb1*^{M318R/+} VSMCs (Fig. 1c–e and Supplementary Table 2). We also noted the upregulation of mechanosensitive transcripts, such as *Thbs1*, *Cyr61/CCN1* and *Ctgf/CCN2* (ref. 20) (Fig. 1e and Supplementary Table 1), suggesting that defective ECM–integrin receptor interactions contribute to induction of mechanical stress responses. Notably, as previously observed in other models of hereditary aortopathy^{21,22}, loss of connections between VSMCs and elastic lamellae could be observed in LDS aortas as early as 6 weeks of age, before severe dilation⁹ (Extended Data Fig. 2).

Additional analysis of transcription factor target databases (ENCODE²³ and Chromatin Immunoprecipitation Enrichment Analysis (ChEA) via EnrichR^{24,25}) showed that the LDS-downregulated transcripts were enriched in targets of nuclear factor erythroid 2-related factor 2, also known as Nrf2, a transcription factor that activates expression of cytoprotective genes and suppresses expression of proinflammatory mediators²⁶ (Fig. 1f and Supplementary Table 2). The targets of the upstream stimulatory factor family, which can modulate the expression of smooth muscle specific genes, were also enriched among downregulated transcripts^{27,28} (Fig. 1f and Supplementary Table 2). Conversely, the target genes for GATA transcription factors and CCAAT enhancer binding protein delta, also known as CEBPD, a positive transcriptional regulator of inflammatory responses mediated by interleukin-1 and interleukin-6 (refs. 29,30), were enriched among transcripts upregulated in LDS VSMCs (Fig. 1g and Supplementary Table 2).

Region- and disease-specific VSMC transcriptional patterns

Given the regional vulnerability observed in LDS aortas, we leveraged insight gained from the literature and scRNA-seq analysis of the aorta of control and *Tgfb1*^{M318R/+} mice to design a custom panel for high

throughput in situ hybridization using the Multiplexed error-robust fluorescence in situ hybridization (MERFISH) spatial transcriptomics platform (Supplementary Table 3). The analysis of a longitudinal section of the proximal aorta of 16-week-old control and LDS mice showed regionally defined expression of several transcripts involved in the modulation of vascular phenotypes (Fig. 2 and Extended Data Fig. 3). The transcripts more highly detected in the aortic root of LDS mice relative to the ascending aorta included *Agtr1a*, which codes for angiotensin II receptor type 1a, a known contributor to LDS pathogenesis, and *Gata4*, which codes for a transcription factor known to positively regulate *Agtr1a* expression in the heart^{31,32}. The transcripts coding for CCAAT enhancer binding protein beta (*Cebpb*), a proinflammatory mediator³³, and maternally expressed gene 3 (*Meg3*), a long noncoding RNA that negatively regulates TGF- β signaling and promotes VSMC proliferation³⁴, were also enriched in this region. In contrast, expression of cardiac mesoderm enhancer-associated noncoding RNA (*Carmn*), a positive regulator of VSMC contractile function that is downregulated in vascular disease, and expression of *Myh11*, coding for a marker of differentiated VSMCs, was enriched in the distal ascending aorta, a region that is only mildly affected in LDS mouse models³⁵.

Spatial distribution of VSMC1/VSMC2-defining transcripts

To examine if the spatial VSMC heterogeneity observed with MERFISH could be captured by scRNA-seq, we increased the clustering resolution for VSMCs, thus obtaining two subclusters, VSMC1 and VSMC2. We then examined the cluster-defining transcripts for these two VSMC subclusters (Supplementary Table 4), for transcripts our laboratory has previously shown to progressively increase (that is, *Tes* and *Ptprz1*) and decrease (that is, *Enpep* and *Notch3*) along the proximal-to-distal axis in the mouse ascending aorta²². Regardless of genotype, VSMC1 and VSMC2 showed differential expression of transcripts whose expression is intrinsically enriched in the ascending aorta and the aortic root, respectively²² (Fig. 3a,b and Supplementary Table 4). *Gata4* was also noted among the transcripts that defined the VSMC2 subcluster and whose expression was highest in the aortic root, progressively diminishing along the proximal-to-distal axis in the ascending aorta, in both control and LDS aortas (Fig. 3c and Extended Data Figs. 4 and 5).

Considering previous work highlighting how cell lineage modulates the effect of LDS-causing mutations^{10,36}, we explore the relationship between the VSMC2 and VSMC1 subclusters to the secondary heart field (SHF) and cardiac neural crest (CNC) lineage of origin (Extended Data Fig. 3). We found that VSMCs lineage-traced with a fluorescent reporter identifying CNC-derived cells were over represented in the VSMC1 subcluster (Extended Data Fig. 6a). However, reanalysis of a previously published dataset of SHF- and CNC-traced VSMCs (Supplementary Table 5) showed that VSMC1 and VSMC2 were not defined by lineage of origin, with VSMCs of both lineages found in either VSMC subcluster³⁷ (Extended Data Fig. 6b). Nevertheless, as would be expected based on the known proximal-to-distal distribution of SHF- and CNC-derived VSMCs, there was overlap between VSMC2-defining and SHF-enriched transcripts (Extended Data Fig. 6b,c and Supplementary Tables 4 and 5). To assess if the VSMC substructure identified in murine models was relevant in the context of human aortic disease, we also reanalyzed a recently published scRNA-seq dataset of aortic tissue from patients with LDS and donor aortas in which the ascending aorta and aortic root were separately sequenced (Fig. 3d and Extended Data Fig. 7)³⁸. The subpopulations of VSMCs expressing cluster-defining transcripts analogous to those found in VSMC1 and VSMC2 in mouse aortas could be identified in the human dataset (Fig. 3d and Supplementary Table 6). Although both VSMC1 and VSMC2 were present in human aortic root and ascending aorta, GATA4 expression was highest in the VSMC2 cluster from the aortic root, with no detectable expression in the ascending aorta (Fig. 3d).

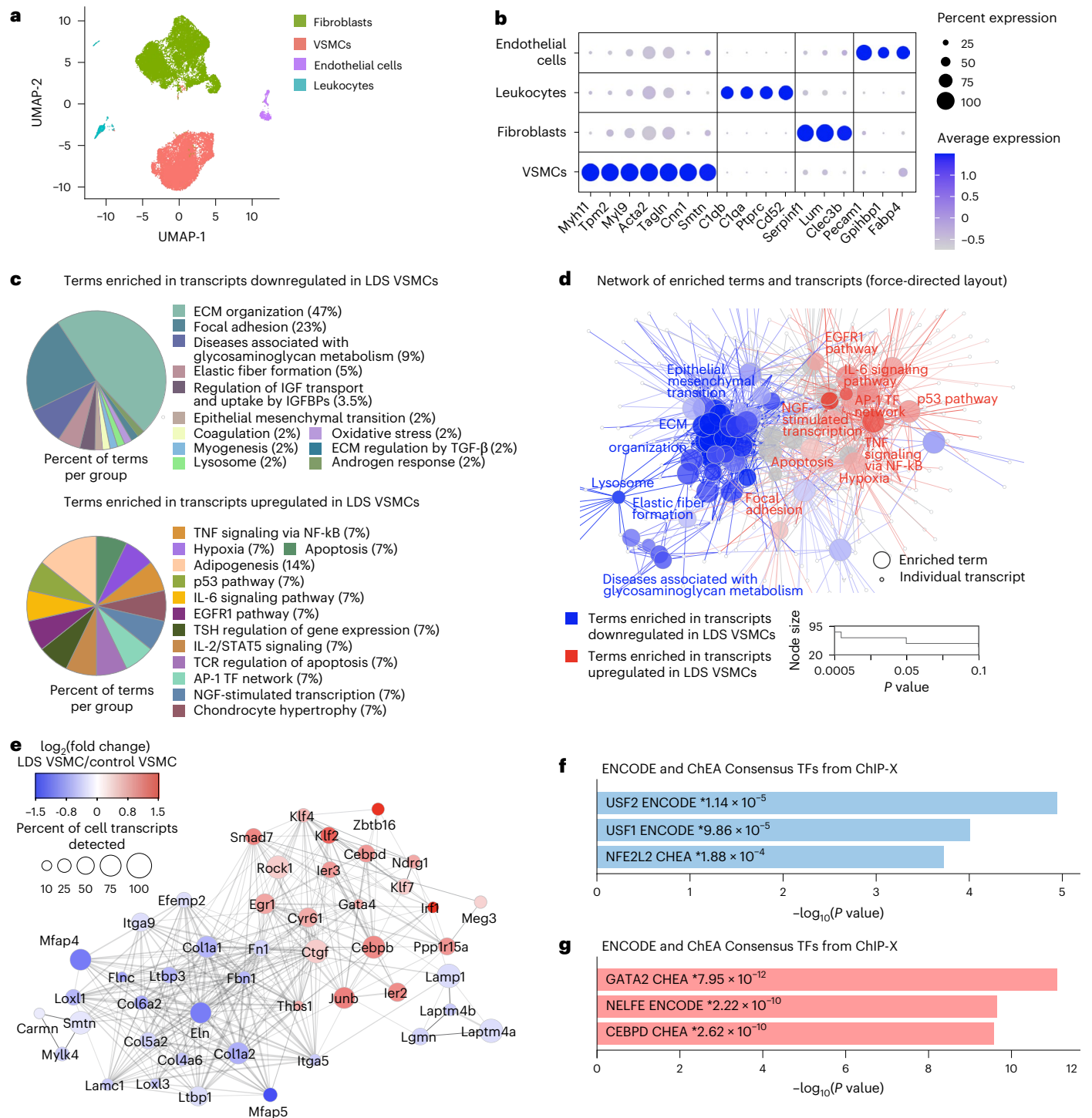


Fig. 1 | Downregulation of transcripts associated with ECM-receptor interactions and upregulation of stress and inflammation pathways in *Tgfbfr1*^{M318R/+} LDS VSMCs. a, A UMAP of aortic cells from control (*Tgfbfr1*^{+/+}) and LDS (*Tgfbfr1*^{M318R/+}) mice. **b**, A dot plot of cluster-defining transcripts used to identify endothelial cells, leukocytes, fibroblasts and VSMCs. The color of the dot represents a scaled average expression, while the size indicates the percentage of cells in which the transcript was detected. **c**, A ClueGO analysis of terms enriched among transcripts up- and downregulated in LDS VSMCs relative to the controls (IGF, insulin growth factor; IGFBP, IGF binding protein; TCR, T cell receptor; NGF, nerve growth factor; and TSH; thyroid stimulating hormone). **d**, A ClueGO network, in which each node represents a term/pathway or individual gene associated with that term. The terms enriched among transcripts downregulated

in LDS VSMCs are highlighted in blue, while those enriched among transcripts upregulated in LDS VSMCs are highlighted in red. The size of the node indicates significance of the enrichment calculated by the ClueGO algorithm. **e**, A network of selected transcripts significantly dysregulated in LDS VSMCs. The size of the node is proportional to the percent of LDS cells in which the transcript was detected. The scale indicates the average \log_2 fold change in expression in LDS VSMCs relative to control VSMCs. The transcripts in blue are decreased in LDS VSMCs, while those in red are increased. **f, g**, EnrichR gene over-representation analysis for the ENCODE and ChEA Consensus transcription factors (TF) library showing the top three most significant terms associated with transcripts that are downregulated (**f**) or upregulated (**g**) in LDS VSMCs. The *P* values (*) refer to the significance of enrichment.

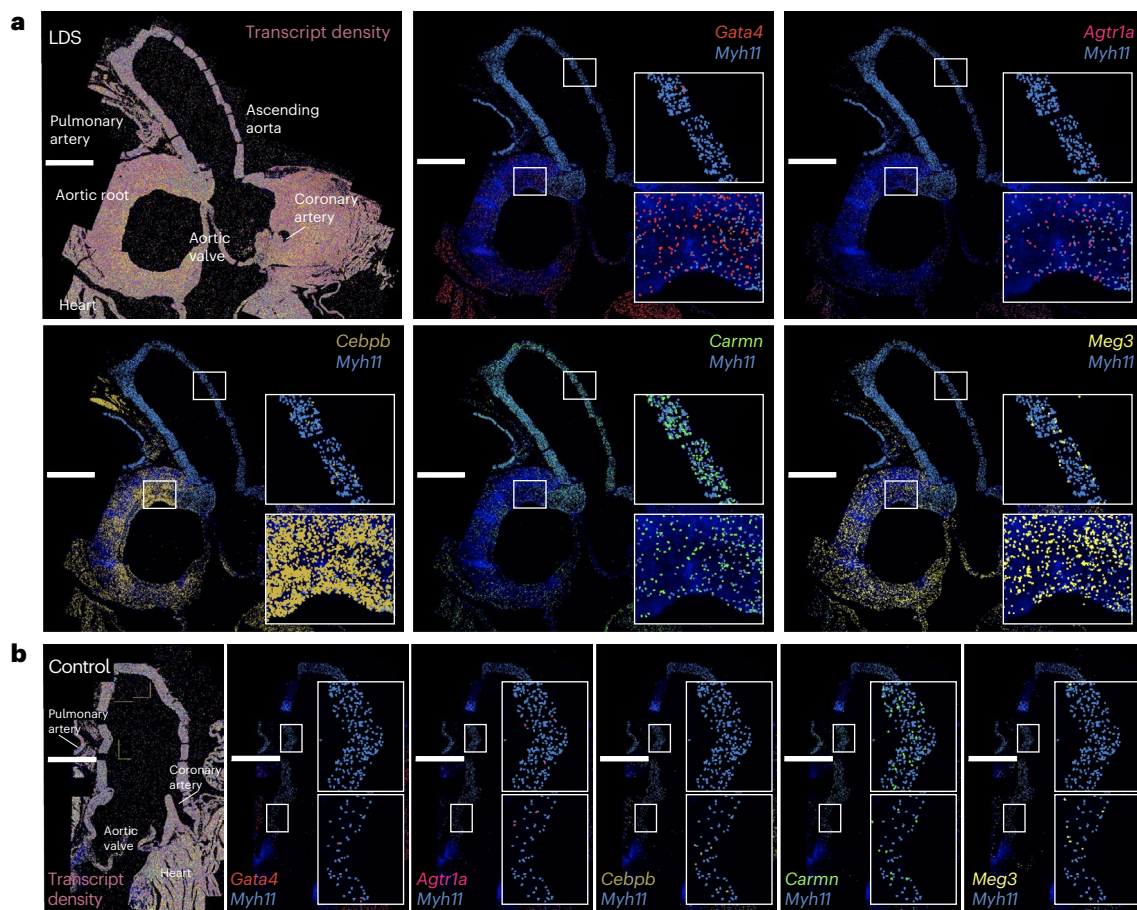


Fig. 2 | MERFISH reveals spatially heterogeneous transcription profiles in LDS VSMCs. a, b, MERFISH images of the proximal aorta of male LDS (**a**) and male control (**b**) mice at 16 weeks of age. Scale bars, 1 mm. The experiment was conducted once on one pair of age- and sex-matched samples. All the detected transcripts across the aortic tissue, with the key anatomic landmarks indicated,

are displayed in **a**, top left. The depiction of the colocalization of *Myh11* and the transcripts of interest are displayed in **a**, top middle, top right, bottom left, bottom middle and bottom right. The insets denote the regions of the ascending aorta and aortic root that are presented at higher magnification.

GATA4⁺ VSMC2 are poised toward a noncontractile phenotype

To examine the biological features of VSMC1 and VSMC2 and whether they were recapitulated in both murine and patient-derived LDS VSMCs, we used the Coordinated Gene Activity in Pattern Sets (CoGAPS) algorithm to identify latent patterns of coordinated gene expression in the *Tgfbri*^{M318R/+} VSMC mouse dataset³⁹. Two patterns, transcriptional patterns 4 and 5, were found to be enriched in the VSMC2 and VSMC1 subclusters, respectively, in the *Tgfbri*^{M318R/+} VSMC mouse dataset (Fig. 3e, g and Supplementary Table 4). These same patterns were then projected onto the scRNA-seq data of VSMCs from the aorta of patients with LDS using ProjectR⁴⁰, revealing a similar enrichment of pattern 4 in VSMC2 and pattern 5 in VSMC1 (Fig. 3e–h, Supplementary Table 4).

As previously observed for transcripts upregulated in *Tgfbri*^{M318R/+} LDS VSMCs, pattern 4-associated transcripts were enriched for transcriptional targets of GATA family members (ENCODE²³ and ChEA dataset, analyzed with EnrichR^{24,25,41,42}; Fig. 3i). Differential gene set enrichment analysis using ClueGO¹⁹ to compare cluster-defining transcripts for VSMC1 and VSMC2 also showed that, in both mouse and human datasets, VSMC2-defining transcripts were enriched for pathways involved in inflammation, senescence and cellular stress (Fig. 3j and Supplementary Tables 7 and 8). In contrast, VSMC1 expressed higher levels of transcripts related to ECM–receptor interactions and contractile function (Fig. 3j, Extended Data Fig. 8 and Supplementary Tables 7 and 8). Network visualization of Molecular Signatures Database (MSigDB) VSMC2-enriched pathways shared by both mouse and human samples (probed with EnrichR^{25,41–44}) (Extended Data Fig. 8a)

and biological terms with shared ClueGO grouping (Fig. 3j and Supplementary Tables 7 and 8), highlighted the biological connections between these pathways and genes over-expressed in VSMC2 relative to VSMC1 (that is, *Cxcl1* (ref. 45), *Irf1* (ref. 46), *Thbs1* and *Gata4* (ref. 47)) (Extended Data Fig. 8b). Overall, in both mouse and human samples, the transcriptional profile of VSMC2 relative to VSMC1 resembled that of less-differentiated VSMCs and included lower expression of *Myh11*, *Cnn1* and *Tet2* and higher expression of transcripts associated with noncontractile VSMC phenotypes, including *Klf4*, *Olfm2*, *Sox9*, *Tcf21*, *Malat1*, *Twist1* and *Dcn*⁴⁸.

GATA4 is upregulated in the aortic root of LDS mice

Based on the analysis described above, including enrichment in GATA-dependent transcription in LDS upregulated transcripts (Fig. 1g) and its known role in driving the upregulation of propathogenic mediators of aneurysm progression, including *Agtr1a*/AT1R³¹, GATA4 emerged as a potential molecular determinant of increased risk of dilation of the aortic root in LDS.

We speculated that the expression of *Gata4* messenger RNA in a subset of VSMC (VSMC2) that are inherently enriched in this region may render these cells more vulnerable to the effects of LDS mutations (Fig. 3c and Extended Data Figs. 4 and 5). Expression of GATA4 mRNA was further upregulated in VSMCs in the LDS aorta, as assessed both by scRNA-seq (Supplementary Table 1) and RNA in situ hybridization (Fig. 4a and Extended Data Fig. 5). Given that expression of GATA4 protein is highly regulated at the post-transcriptional level through

targeted degradation^{47,49}, including via mechanosensitive pathways⁴⁹, we also examined expression of GATA4 protein in control and LDS aortic samples and found that protein expression was increased in LDS aortic root, both by immunofluorescence and immunoblot assays (Fig. 4b,c, Extended Data Fig. 5b and Fig. 5).

Deletion of *Gata4* in VSMC reduces aortic root dilation

To assess whether increased GATA4 levels in aortic root of LDS mouse models promoted dilation in this location, we crossed conditional *Gata4*^{fl^{ox}/fl^{ox}} mice⁵⁰ to LDS mice also expressing a transgenic, tamoxifen-inducible Cre recombinase under the control of a VSMC-specific promoter (*Myh11*-Cre^{ER})⁵¹. GATA4 deletion was induced starting at 6 weeks of age to bypass any potential role of this transcription factor during perinatal aortic development, during which rapid ECM remodeling occurs in conjunction with an increase in systolic pressure and cardiac output⁵² (Fig. 5). As *Myh11*-Cre^{ER} is integrated on the Y chromosome, only male mice were used for this set of experiments.

As expected, control LDS animals (*Tgfb1*^{M318R/+}; GATA4^{Ctrl}) developed progressive focal dilation of the aortic root (albeit not reaching the 150% threshold of the normal diameter required for a definition of aneurysm) (Fig. 6a). This dilation was reduced in LDS mice with VSMC-specific postnatal deletion of GATA4 (*Tgfb1*^{M318R/+}; GATA4^{SMcKO}) (Fig. 6a and Supplementary Table 9). The reduced aortic diameters also correlated with amelioration of aortic root medial architecture relative to control LDS aortas at 16 weeks of age (Fig. 6b). No notable dilation was observed in the ascending aorta of *Tgfb1*^{M318R/+} mice at 16 weeks of age, and GATA4 deletion had no effect on the diameter of this aortic segment (Extended Data Fig. 9a). GATA4 deletion in VSMCs also did not associate with changes in blood pressure (Extended Data Fig. 9b).

Previous work has shown that GATA4 binds to the *Agtr1a* promoter, inducing its expression in heart tissue^{31,32}, and that *Agtr1a* is transcriptionally upregulated in the aortic root of LDS mice, resulting in upregulation of AT1R, which exacerbates LDS vascular pathology^{9,10,32}. Accordingly, GATA4 deletion associated with reduced expression of *Agtr1a* in the aortic root of LDS mice (Fig. 7). Similarly, deletion of GATA4 reduced the expression of *Cebpb* and *Cebpd* (Fig. 8 and Extended Data Fig. 10), which code for proinflammatory transcription factors regulated by and/or interacting with GATA4 in other contexts^{30,33}, which were upregulated in VSMCs in the presence of LDS mutations (Figs. 1 and 2 and Supplementary Table 1).

Discussion

LDS is a hereditary connective tissue disorder characterized by skeletal, craniofacial, cutaneous, immunological and vascular manifestations, including a high risk for aggressive arterial aneurysms². It is caused by mutations that impair the signaling output of the TGF- β pathway, leading to defective transcriptional regulation of its target genes³⁻⁷. Although loss-of-signaling initiates vascular pathology, compensatory upregulation of positive modulators of the pathway results in a 'paradoxical' increase in activation of TGF- β -signaling mediators (that is, phosphorylated Smad2 and Smad3) and increased expression of target genes in diseased aortic tissue of both patients with LDS and

mouse models^{3,5,6,8-10}. This secondary upregulation depends, in part, on increased activation of angiotensin II signaling via AT1R, which positively modulates the expression of TGF- β ligands and TGF- β receptors⁵³. Whereas upregulation of the TGF- β pathway can have both adaptive and maladaptive consequences depending on disease stage and cellular context⁵³, upregulation of AT1R signaling has consistently been shown to be detrimental to vascular health, and both pharmacological (that is, with angiotensin receptor blockers) and genetic antagonism of this pathway ameliorates vascular pathology in LDS mouse models^{53,54}.

Even though LDS-causing mutations confer an increased risk of disease across all arterial segments, the aortic root is one of the sites that is particularly susceptible to aneurysm development¹¹⁻¹³. In this study, we leverage scRNA-seq in conjunction with spatial analysis via high throughput in situ hybridization to investigate the heterogeneity of VSMCs in an LDS mouse model, with the ultimate goal of identifying regional mediators that may drive upregulation of proathrogenic signaling in this region. We identify distinct subpopulations of VSMCs characterized by expression patterns that preferentially map to the ascending aorta (VSMC1) and aortic root (VSMC2) in mouse aorta. We also show that the regional vulnerability of the aortic root depends, in part, on higher levels of *Gata4* expression in a subset of VSMCs (VSMC2), which is intrinsically more vulnerable to the effect of an LDS-causing mutation.

Before the advent of single-cell analysis tools, which allow precise and unbiased unraveling of cellular identity, the ability to investigate VSMC heterogeneity in the proximal aorta was limited by the availability of experimental approaches to investigate known or expected diversity. In consideration of the mixed embryological origin of the aortic root and distal ascending aorta, earlier work, thus, focused on understanding how the effect of LDS mutations on VSMCs was modified by the SHF and CNC lineage of origin. In both mouse models and in induced pluripotent stem cell-derived in vitro models, signaling defects caused by LDS mutations were found to be more pronounced in VSMC derived from SHF (or cardiac mesoderm) progenitors relative to CNC-derived VSMCs^{10,36}.

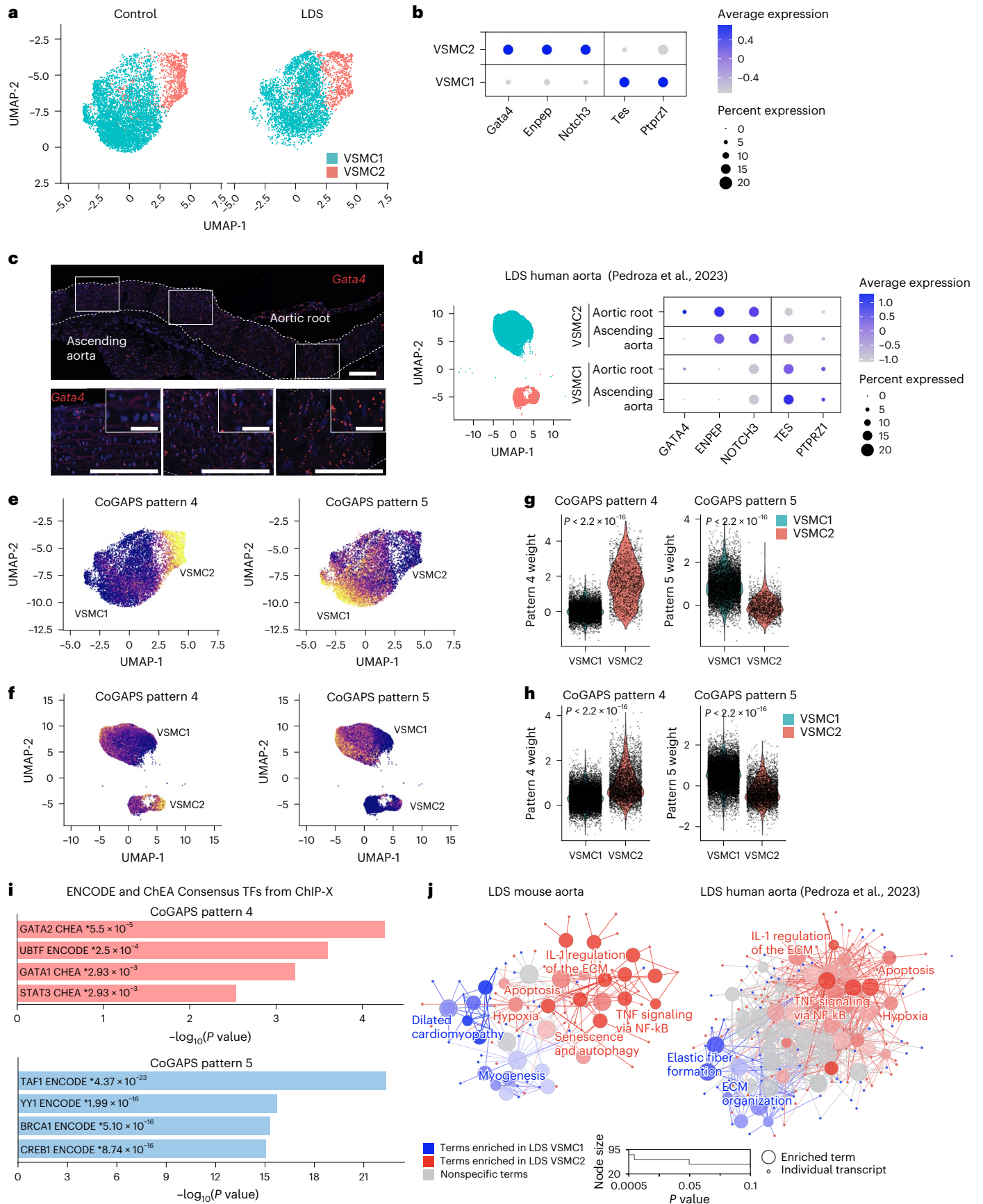
Similar to SHF-derived VSMCs, *Gata4*-expressing VSMC2 are enriched in the aortic root and are also more vulnerable to the effects of an LDS-causing mutation. They also express a transcriptional signature similar to that of SHF-derived VSMCs (Extended Data Fig. 3). Reciprocally, SHF-derived cells are over represented in the VSMC2 cluster in our dataset (Extended Data Fig. 3). However, the identity of VSMC2 and VSMC1 is not defined by lineage of origin, and the SHF- or CNC-derived origin is only an imperfect approximation of the VSMC heterogeneity that can now be assessed via scRNA-seq.

Heterogeneity beyond that imposed by lineage of origin was also shown by scRNA-seq analysis of the aorta of the *Fbn1*^{C1041G/+} Marfan syndrome mouse model, which revealed the existence of an aneurysm-specific population of transcriptionally modified smooth muscle cells at a later stage of aneurysmal disease and which could emerge from modulation of both SHF- and non-SHF (presumably CNC)-derived progenitors^{37,55}. These cells, which could also be identified in the aneurysmal tissue derived from the aortic root of patients

Fig. 3 | Transcriptionally and spatially defined VSMC subclusters with distinct responses to LDS-causing mutations can be identified in both murine and human aortas. a, A UMAP of VSMCs from control (*Tgfb1*^{+/+}) and LDS (*Tgfb1*^{M318R/+}) mice shown split by genotype. b, A dot plot showing enrichment of cluster-defining transcripts in VSMC1 and VSMC2. For a given transcript, the color of the dot represents a scaled average expression, while the size indicates the percentage of cells in which it was detected. c, RNA in situ hybridization showing the expression of GATA4 along the length of the murine aorta in a 16-week-old control animal, representative of five independent biological replicates. Bottom: the insets identify the location shown at a higher magnification. The dashed line identifies the approximate boundaries of the aortic wall. Scale bars, 100 μ m. d, A UMAP of control and LDS VSMCs from

human patients and a dot plot of cluster-defining markers in this dataset split by aortic region (Pedroza et al.³⁸). e, f, A UMAP overlaid with weights for CoGAPS patterns 4 and 5, in mouse (e) and human (f) scRNA-seq datasets. g, h, Violin plots showing the distribution of pattern 4 and 5 weights in VSMC subclusters from mouse (g) and human (h) scRNA-seq datasets. The *P* values refer to Wilcoxon test. i, An EnrichR gene over-representation analysis for the ENCODE and ChEA Consensus transcription factor (TF) library showing the top four most significant terms associated with transcripts that define CoGAPS patterns 4 and 5. The *P* values (*) refer to the significance of enrichment. j, ClueGO network of terms differentially enriched in mouse and human LDS VSMC2 relative to VSMC1. The terms highlighted in blue are enriched in VSMC1, while those highlighted in red are enriched in VSMC2.

human patients and a dot plot of cluster-defining markers in this dataset split by aortic region (Pedroza et al.³⁸). e, f, A UMAP overlaid with weights for CoGAPS patterns 4 and 5, in mouse (e) and human (f) scRNA-seq datasets. g, h, Violin plots showing the distribution of pattern 4 and 5 weights in VSMC subclusters from mouse (g) and human (h) scRNA-seq datasets. The *P* values refer to Wilcoxon test. i, An EnrichR gene over-representation analysis for the ENCODE and ChEA Consensus transcription factor (TF) library showing the top four most significant terms associated with transcripts that define CoGAPS patterns 4 and 5. The *P* values (*) refer to the significance of enrichment. j, ClueGO network of terms differentially enriched in mouse and human LDS VSMC2 relative to VSMC1. The terms highlighted in blue are enriched in VSMC1, while those highlighted in red are enriched in VSMC2.



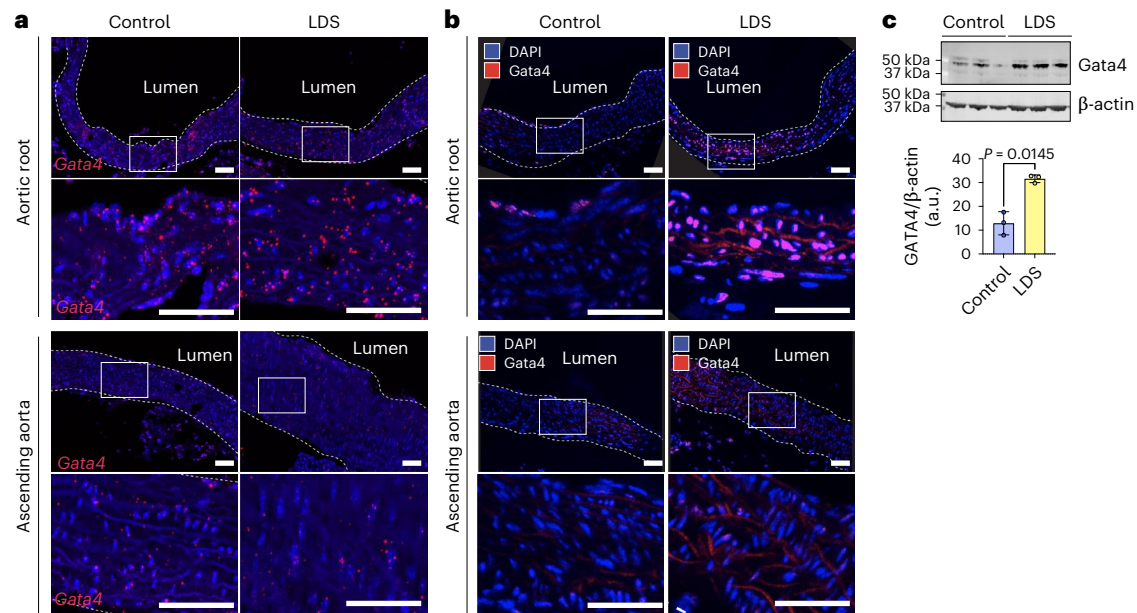


Fig. 4 | GATA4 mRNA and protein are upregulated in the aortic root of LDS mice. **a**, An RNA in situ hybridization for *Gata4* in the aortic root and ascending aorta of control and LDS (*Tgfbri*^{M318R/+}) male mice; the images are representative of five independent biological replicates. Bottom: the insets identify the location shown at higher magnification. Scale bars, 50 and 200 μ m, respectively. **b**, Immunofluorescence for GATA4 in the aortic root and ascending aorta of control and LDS mice; the images are representative of five independent biological replicates. Bottom: the insets identify the location shown at higher

magnification. Scale bars, 50 and 200 μ m, respectively. The dashed line approximates the boundary of the aorta. **c**, An immunoblot for GATA4 expression relative to β -actin in aortic root lysates of control ($n = 3$ independent biological replicates), LDS mice ($n = 3$ independent biological replicates) and the related quantification of the immunoblot. The *P* value refers to a two-tailed Welch's *t*-test ($t = 6.32$, d.f. = 2.43). Each symbol represents an independent biological replicate, and the bar graph shows the mean \pm standard deviation.

with Marfan syndrome, showed a transcriptional signature marked by a gradual upregulation of ECM genes and downregulation of VSMC contractile genes^{37,55}. We were not able to identify this population of modified smooth muscle cells in the aorta of *Tgfbri*^{M318R/+} LDS mouse models, even though it was shown to exist in the aorta of patients with LDS⁴⁰.

Similar to the early effect of Smad3-inactivation, the *Tgfbri*^{M318R/+} LDS mutation caused broad downregulation of gene programs required for ECM homeostasis and those favoring a differentiated VSMC phenotype²² (Fig. 1); conversely, proinflammatory transcriptional repertoires, with an enrichment in terms related to hypoxia, p53-dependent pathways and mechanical stress, were observed among upregulated transcripts. We speculate that this latter profile represents a response to loss of connections between VSMCs and elastic lamellae, which can be observed as early as 6 weeks of age (Extended Data Fig. 2) and is probably caused by decreased expression of ECM components whose expression requires TGF- β /Smad activity¹⁷.

We also noted downregulation of several components of the lysosome, whose function is required for cellular homeostasis and degradation of protein targets via selective autophagy⁵⁶ (Fig. 1). GATA4 levels are regulated via p62-mediated selective autophagy⁴⁷ and by mechanosensitive proteasome-mediated degradation^{49,57}. The aortic root would be especially vulnerable to a defect in either of these processes given increased baseline levels of *Gata4* mRNA expression in VSMC2. Increased levels of GATA4 may contribute to vascular pathogenesis by several potential mechanisms. In other cellular contexts, GATA4 has been shown to promote induction of the proinflammatory senescence-associated secretory phenotype, as well as transcription of the long noncoding RNA *Malat1*, which promotes aneurysm development in other mouse models⁵⁸. GATA4 is also a negative regulator of contractile gene expression in Sertoli and Leydig cells⁵⁹. In addition, GATA4 binds the promoter and activates the expression of *Agtr1a*³¹, which is known to drive proathrogenic signaling in LDS aorta³².

Accordingly, we find that GATA4 deletion downregulates expression of *Agtr1a* in the aortic media of LDS mouse models (Fig. 7).

Reanalysis of a scRNA-seq dataset of human aortic samples from patients with LDS, which included both the aortic root and the ascending aorta, shows that a population of *Gata4*-expressing VSMCs, similar to that found in mice, can also be identified in patients with LDS. In addition, patterns of coordinated gene expression identifying VSMC1 and VSMC2, which were learned from the scRNA-seq analysis of mouse aorta, could be projected onto the human dataset, suggesting that these two subsets of VSMCs are conserved across species and that the existence of a *Gata4*-expressing VSMC2 population may underlie increased risk in the aortic root of patients with LDS as well. Our study supports the notion that GATA4 is a factor sensitizing the aortic root to the effects of LDS mutations and that its inhibition early in the disease process reduces the rate of dilation. However, it is likely that, as for treatment with AT1R signaling inhibitors⁶⁰, the beneficial effect of inhibiting this transcription factor will diminish at later stages of disease.

GATA4 is an important factor in aortic valve development and noncoding and missense variants in *GATA4* have been implicated in patients with bicuspid aortic valve disease^{61,62}. It also plays critical roles in regulation of numerous biological processes in nonvascular tissues^{63,64}, making its direct targeting for therapeutic purposes unfeasible. However, this work highlights how the investigation of factors that increase or decrease the regional risk of aortic aneurysm may lead to a better understanding of adaptive and maladaptive pathways activated in response to a given aneurysm-causing mutation. This knowledge may be leveraged to develop therapeutic strategies that target the vulnerabilities of specific arterial segments.

Methods

All animal experiments were conducted according to protocols (approval number MO22M307) approved by the Johns Hopkins University School of Medicine Animal Care and Use Committee.

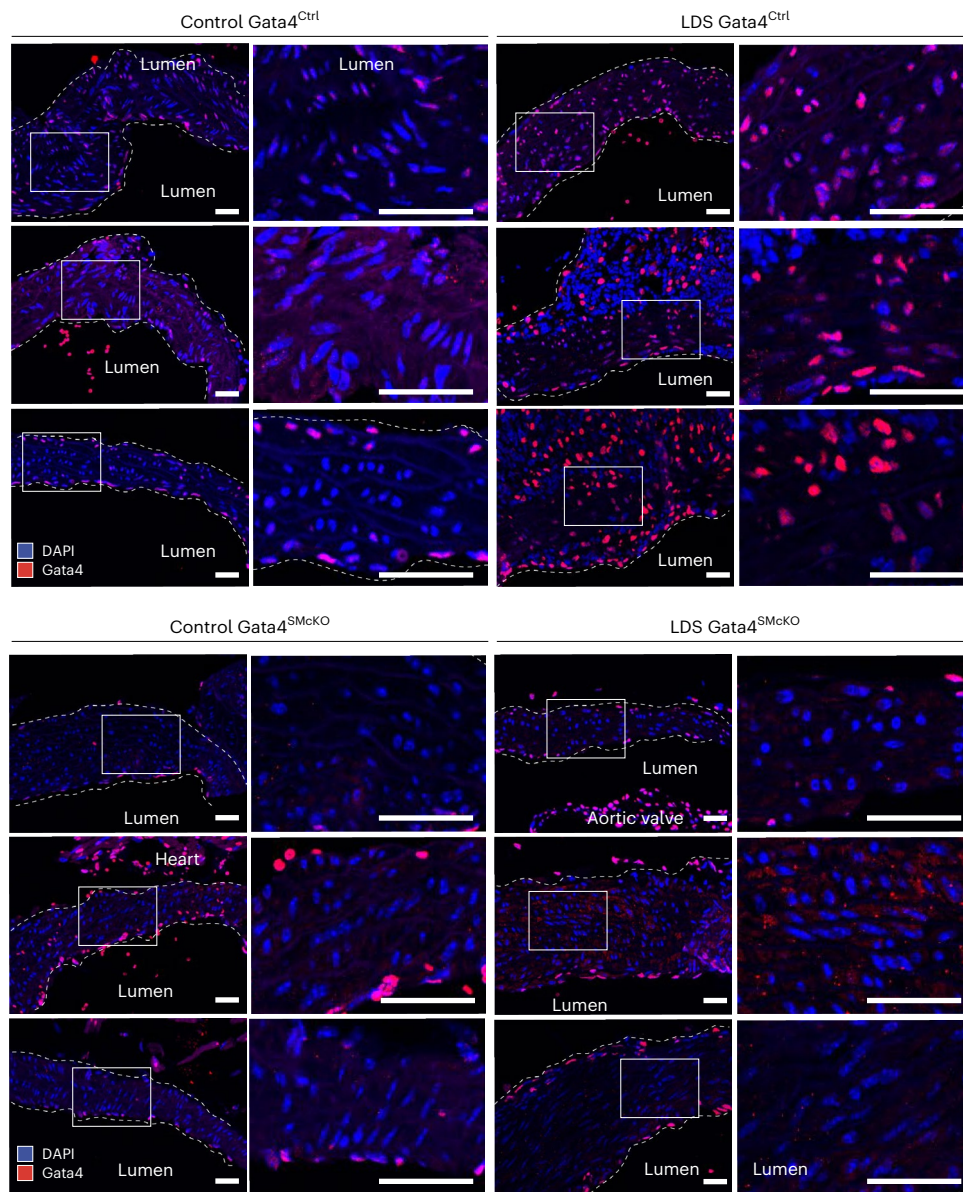


Fig. 5 | GATA4 protein is upregulated in LDS aortic root of GATA4^{Ctrl} and effectively ablated in GATA4^{SMcKO} mice. The immunofluorescence for GATA4 in the aorta of male mice of the indicated genotype at 16 weeks of age is shown. Three independent biological replicates are shown per genotype, abbreviated as follows: control (*Tgfb1*^{+/+}) and LDS (*Tgfb1*^{M318R/+}) with (GATA4^{SMcKO}) or without

(GATA4^{Ctrl}) smooth muscle specific deletion of GATA4. The insets identify the location shown at a higher magnification. The images were acquired at 20× magnification. Scale bars, 50 and 200 μm, respectively. The dashed line approximates the boundary of the aorta.

Animal experiments

All mice were maintained in an animal facility at 72 °F and 40–60% humidity. The mice were provided unlimited access to standard chow and water and a light–dark cycle of 10–14 h. *Tgfb1*^{+/+} and *Tgfb1*^{M318R/+} (ref. 9) (The Jackson Laboratory, strain no. 036511) mice, some bearing the *EGFP-L10a* (The Jackson Laboratory, strain no. 024750) conditional tracer allele and a CNC-specific Cre recombinase expressed under the control of Wnt2 promoter (The Jackson Laboratory, strain no. 003829) were used for scRNA-seq as described below. All mice were maintained on a 129-background strain (Taconic, 129SVE). *Tgfb1*^{+/+} and *Tgfb1*^{M318R/+} mice were bred to *Gata4*^{fllox/fllox} (The Jackson Laboratory, strain no. 008194) and mice carrying the *Myh11-Cre^{ER}* transgene (The Jackson Laboratory, strain no. 019079). *Myh11-Cre^{ER}* is integrated on the Y chromosome; therefore, only male mice were used for this set of experiments. *Tgfb1*^{+/+} and *Tgfb1*^{M318R/+} bearing *Gata4*^{fllox/fllox} and *Myh11-Cre^{ER}* are referred to as GATA4^{SMcKO}. *Tgfb1*^{+/+} and *Tgfb1*^{M318R/+}

bearing *Gata4*^{+/+} with or without *Myh11-Cre^{ER}* or *Gata4*^{fllox/fllox} or *Gata4*^{fllox/+} without *Myh11-Cre^{ER}* are referred to as GATA4^{Ctrl}. All GATA4^{SMcKO} and GATA4^{Ctrl} mice were injected with 2 mg per day of tamoxifen (MilliporeSigma, T5648) starting at 6 weeks of age for five consecutive days. The mice were genotyped according to The Jackson Laboratory protocols for these models. Serial echocardiography was performed using the Visual Sonics Vivo 2100 machine and a 30 MHz probe. As there is some variability in the onset of aortic dilation in *Tgfb1*^{M318R/+} mice and starting aortic size will affect final measurements, an aortic root diameter of 1.9 mm and above at baseline (8 weeks of age) was defined a priori as an exclusion criterion.

Molecular validation techniques

Aortic sample preparation. All mice were euthanized by halothane inhalation at a 4% concentration, 0.2 ml per liter of container volume (MilliporeSigma, H0150000). The heart and thoracic aorta

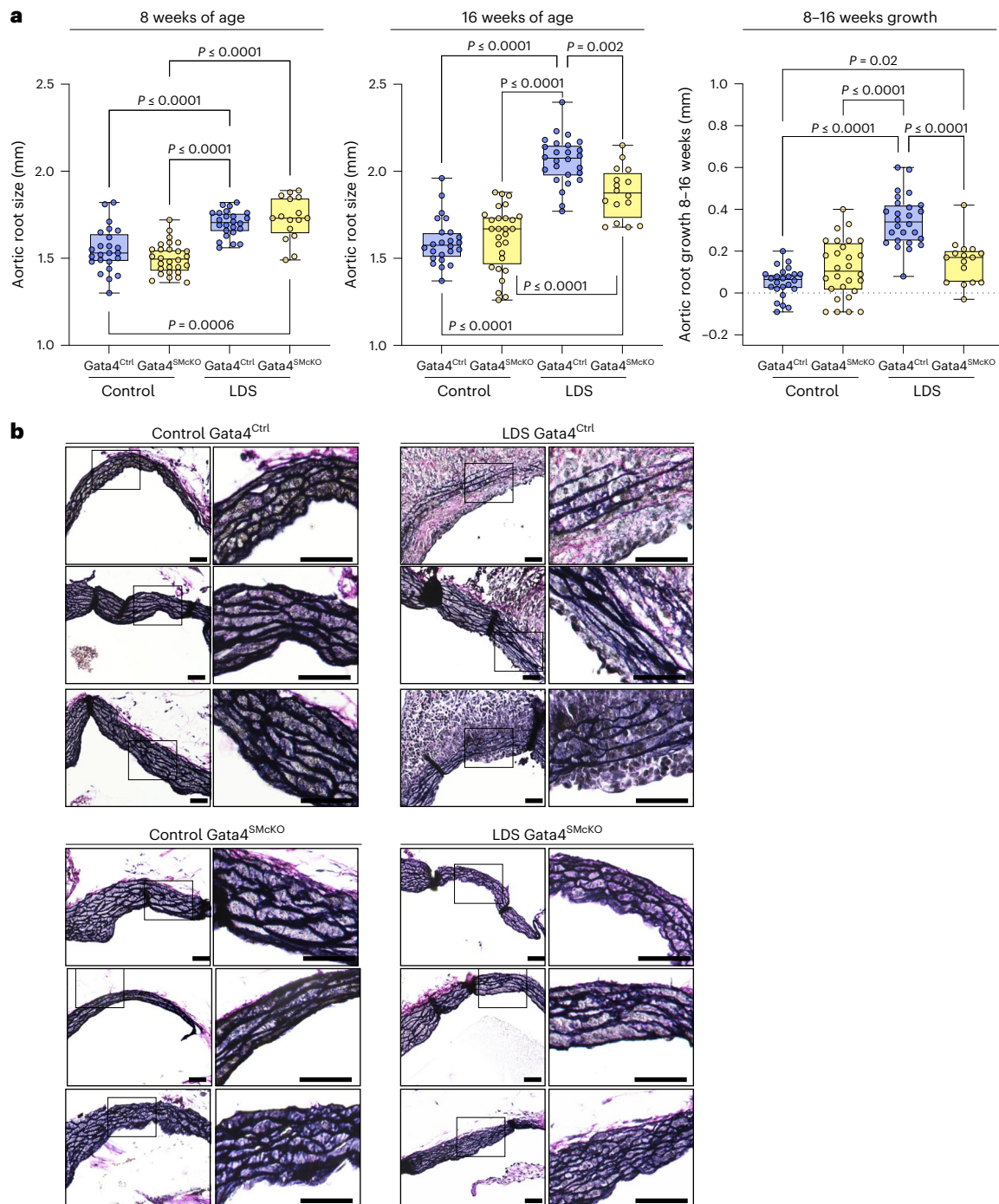


Fig. 6 | Smooth-muscle-specific deletion of GATA4 (GATA4^{SMcKO}) reduces aortic root size and growth and improves aortic root media architecture in LDS mice. a, Aortic root diameter of male control (*Tgfb1*^{+/+}) and LDS (*Tgfb1*^{M31SR/+}) with GATA4^{SMcKO} or without (GATA4^{Ctrl}) smooth muscle specific deletion of GATA4, as measured by echocardiography at 8 and 16 weeks of age and aortic root growth from 8 to 16 weeks of age. The box plots show the upper quartile, median and lower quartile; each symbol represents an independent biological replicate. The whiskers identify the minimum to maximum range

(control GATA4^{Ctrl} $n = 24$; control GATA4^{SMcKO} $n = 28$; LDS GATA4^{Ctrl} $n = 26$; LDS GATA4^{SMcKO} $n = 16$). The P values refer to Brown–Forsythe ANOVA (8 weeks: F^* (F-statistic) = 25.98, DFn (degrees of freedom numerator) of 3, Dfd (degrees of freedom denominator) of 66.69; 16 weeks: $F^* = 55.54$, DFn of 3, Dfd of 82.30; 8–16 weeks: $F^* = 33.39$, DFn of 3, Dfd of 78.63). **b**, VVG-stained aortic root sections from three independent biological replicates per genotype. The insets identify the area shown at a higher magnification. Scale bars, 50 and 200 μ m, respectively.

were dissected en bloc and fixed in 4% paraformaldehyde (Electron Microscopy Sciences, 15710) in PBS at 4 °C overnight. The samples were subsequently incubated in 70% ethanol at 4 °C overnight before embedding in paraffin. Paraffin-embedded tissues were cut into 5 μ m sections to expose a longitudinal section of the thoracic aorta. The sections were then stained with Verhoeff–van Gieson (StatLab, STVG1) to visualize

elastic fiber morphology or to assess protein and RNA abundance by immunofluorescence or fluorescence in situ hybridization.

Immunofluorescence. Immunofluorescence was performed following a protocol adapted from Cell Signaling Technology (CST) for formaldehyde-fixed tissues. The paraffin-embedded sections

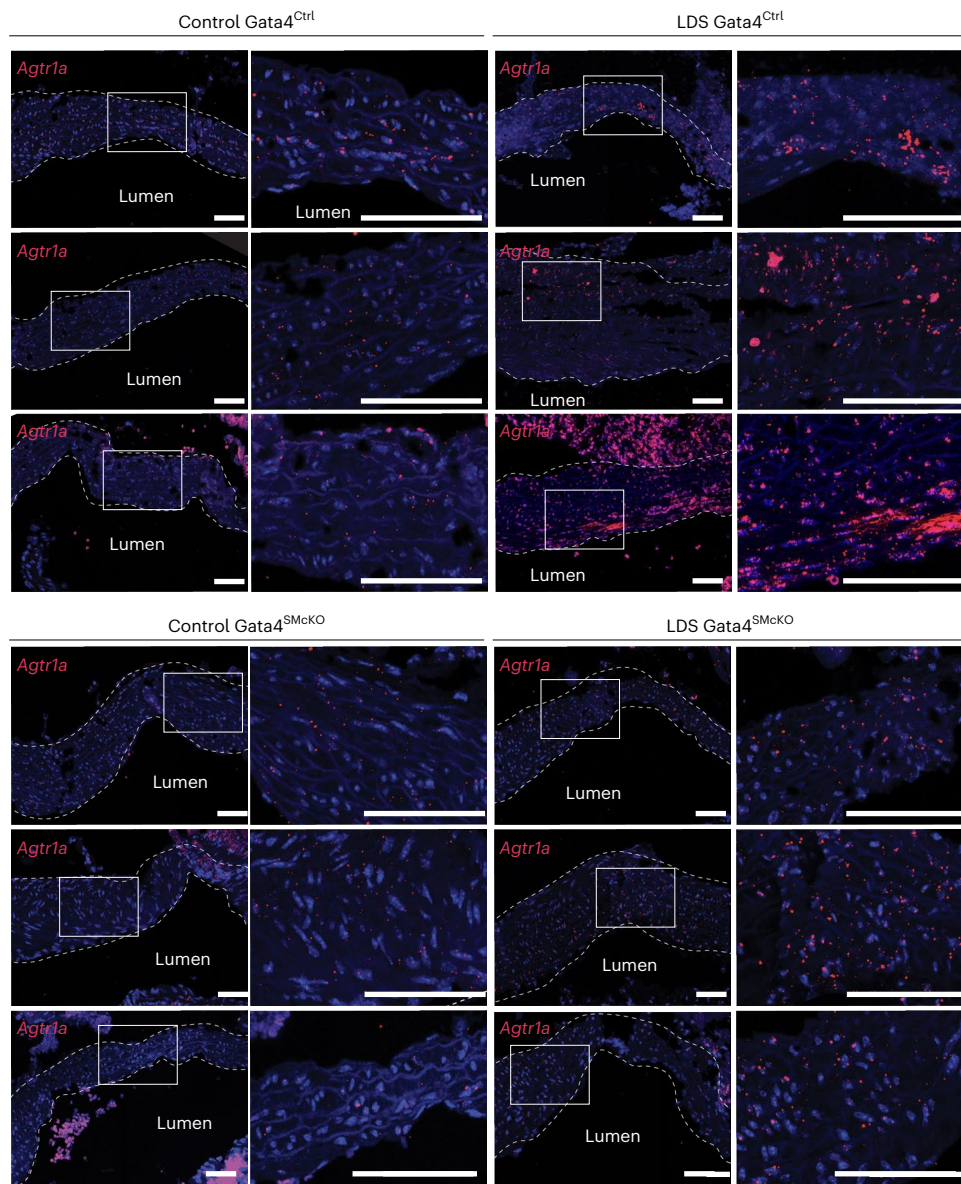


Fig. 7 | Smooth muscle-specific deletion of GATA4 results in reduced expression of *Agtr1a*. RNA in situ hybridization for *Agtr1a* in the aortic root of mice of the indicated genotype at 16 weeks of age. Three independent biological replicates are shown per genotype, abbreviated as follows: control (*Tgfbri*^{+/+}) and LDS (*Tgfbri*^{M318R/+}) with (GATA4^{SMcKO}) or without (GATA4^{Ctrl}) smooth-muscle-

specific deletion of GATA4. The insets identify the location shown at a higher magnification. The images were acquired at 20× magnification. Scale bars, 50 and 200 μm, respectively. The dashed line approximates the boundary of the aorta.

were baked at 60 °C for 15 min, then deparaffinized in xylene followed by rehydration via a graded alcohol series: 100% ethanol, 95% ethanol, 70% ethanol and 1× PBS, each for 3 min. An antigen retrieval was performed in 10 mM sodium citrate buffer (0.05% Tween, pH 6.0) at 90 °C for 15 min. The slides were allowed to cool to room temperature before the sections were treated with 10 mg ml⁻¹ sodium borohydride in PBS (Sigma-Aldrich, 452882) for 20 min. The slides were permeabilized in Tris-buffered saline with Triton X-100 (TBT) (1× Tris-buffered saline (TBS) (Quality Biological, 351086101) with 0.1% Triton X-100 (Sigma-Aldrich, T9284) and 0.1 M glycine (Sigma-Aldrich, G8898)) for 20 min, followed by blocking with Fc Receptor Blocker (Innovex, NB309) and Background Buster (Innovex, NB306), each for 20 min at room temperature. The slides were then incubated with GATA4 antibody (CST, CST36966) diluted 1:100 in TBT overnight at 4 °C in a humid chamber. Following two washes with TBT, the slides were treated with donkey anti-rabbit Alexa Fluor 555 (ThermoFisher, A32794) at 1:100 for 1 h. The slides were washed again twice with TBT

and once with TBS before mounting with Hard Set Mounting Media with 4,6-diamidino-2-phenylindole (DAPI) (VECTASHIELD, H-1500). The images were taken using a Zeiss LSM880 Airyscan FAST confocal microscope at 20× magnification and are presented as maximal intensity projection.

RNAscope fluorescence in situ hybridization. RNA in situ hybridization was performed using the RNAscope Multiplex Fluorescent Reagent Kit v2 Assay (ACD Biosciences, 323100) according to the manufacturer's protocol with the following probes *Mm-Gata4* (417881), *Mm-Agtr1a* (481161), *Mm-Cebpd* (556661) and *Mm-Cebpb* (547471). The images were taken using a Zeiss LSM880 Airyscan FAST confocal microscope at 20× magnification and are presented as maximal intensity projection.

Immunoblotting. Aortic root tissue was flash-frozen immediately upon dissection and stored at -80 °C until protein extraction. The protein was extracted using Full Moon Lysis Buffer (Full Moon Biosystems,

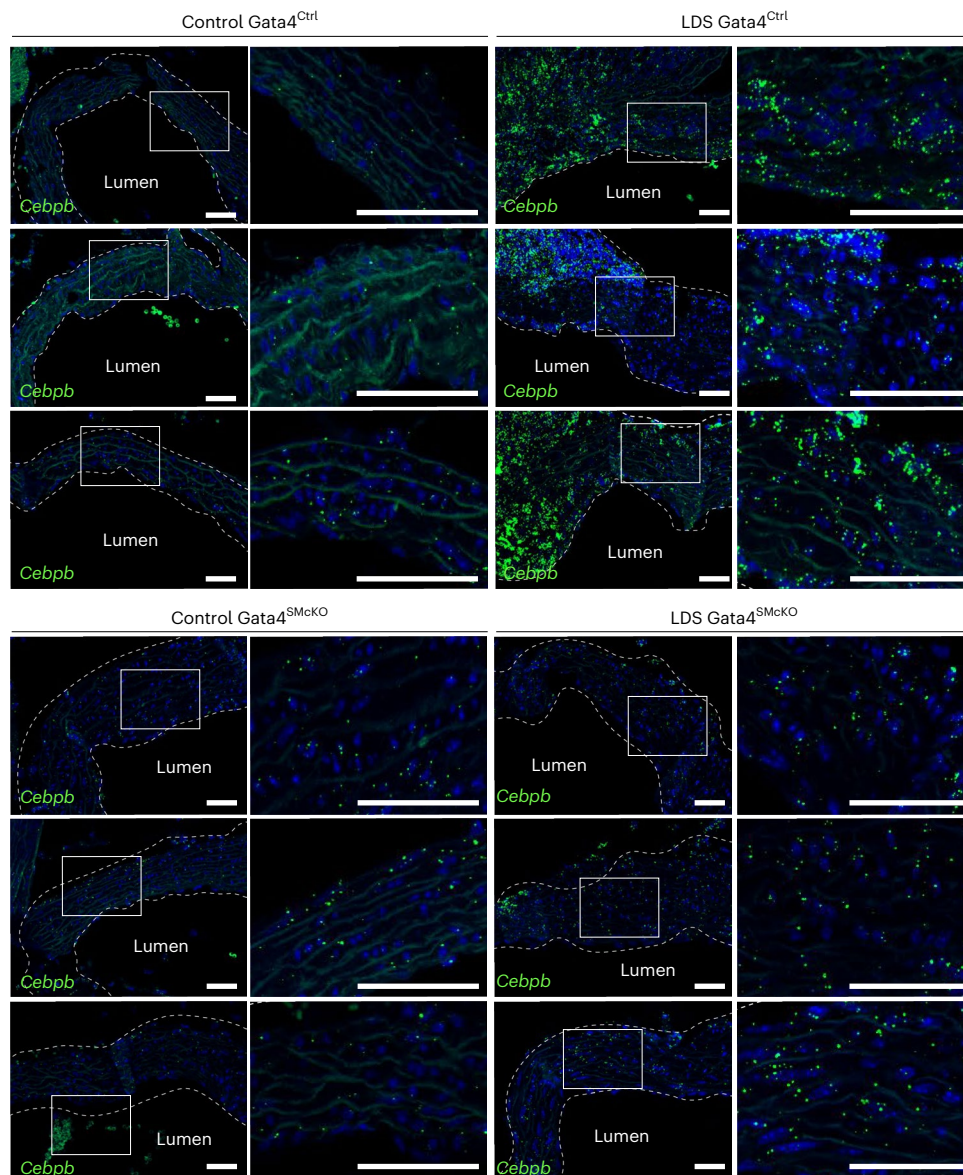


Fig. 8 | Smooth-muscle-specific deletion of GATA4 results in reduced expression of *Cebpb*. RNA in situ hybridization for *Cebpb* in the aortic root of mice of the indicated genotype at 16 weeks of age. Three independent biological replicates are shown per genotype, abbreviated as follows: control (*Tgfbri*^{+/+}) and LDS (*Tgfbri*^{M318R/+}) with (GATA4^{SMcKO}) or without (GATA4^{Ctrl}) smooth-muscle-

specific deletion of GATA4. The insets identify the location shown at a higher magnification. The images were acquired at 20× magnification. Scale bars, 50 and 200 μm, respectively. The dashed line approximates the boundary of the aorta.

EXB1000) with added phosphatase and protease inhibitors (Millipore-Sigma, 11836170001 and 4906845001) and Full Moon lysis beads (Full Moon Biosystems, LB020) using an MP Biomedicals FastPrep 24 5G automatic bead homogenizer. After homogenization, the cell debris was pelleted, and the supernatant was collected. The samples were run on a 4–12% Bis-Tris Criterion XT gel (BioRad, 3450123) for 1.5 h at 100 V. The BioRad Turbo Blot standard 30 min protocol was used for transferring to a polyvinylidene difluoride membrane (BioRad, 1704273). The membrane was blocked for 45 min in diluted blocking buffer in PBS (LI-COR, 927-70003) for 1 h at room temperature. The primary antibodies for GATA4 (CST, CST36966) diluted 1:1,000 in blocking buffer and β-actin diluted 1:5,000 in blocking buffer (CST, CST3700) were incubated overnight at 4 °C. The membrane was washed with PBST (1× PBS + 0.05% Tween20) three times for 5 min each. The membrane was incubated with secondary antibodies (LI-COR 926-68072 and 926-32213) diluted 1:10,000 in blocking buffer. The membrane was washed

three more times in PBST, then twice with 1× PBS and imaged on the LI-COR Odyssey machine.

Electron microscopy. The heart and thoracic aorta were prepared en bloc for electron microscopy. The samples were fixed in a solution of sodium cacodylate (0.1 M) and 4% paraformaldehyde (Electron Microscopy Sciences, 15710) overnight at 4 °C. They were then incubated in a 30% sucrose solution overnight at 4 °C. The samples were embedded in optimal cutting temperature compound then stored at –80 °C to freeze completely. The blocks were cut into 20 μm sections using a cryostat and mounted on slides. The clearest longitudinal cross sections of the thoracic aorta were selected and fixed with 2.5% glutaraldehyde solution, followed by a solution of 2% osmium in cacodylate buffer. These sections were then embedded in Epoxy resin (EPON), and the regions of interest—the aortic root and ascending aorta—were cut out. The sections of these regions, 60 nm, were then triple stained with

tannic acid, uranyl acetate and lead citrate. The images were acquired by Johns Hopkins School of Medicine microscope facility staff on a ThermoFisher Talos L120CG2 Electron microscope with a 16 megapixel CMOS camera at 120 Kv.

Transcriptomic analyses

scRNA-seq and analysis. The single-cell suspensions from each mouse were processed separately using the 10x Genomics 3' v3 platform and sequenced on an Illumina NovaSeq. A total of 30,704 aortic cells were sequenced from six female mice. The raw data were processed, aligned to the mouse genome (mm10) and aggregated using 10x Genomics Cell Ranger V6. The data were then filtered using the Seurat V5 package based on the following criteria: >1,000 transcripts detected per cell but <5,000 and >1,500 total molecules detected per cell but <25,000 and <20% mitochondrial transcripts per cell. Filtering reduced this dataset from 30,704 aortic cells to 24,971 cells for further analysis. The data were then normalized using the function SCTransform v2. As samples were prepared on multiple days, the data were integrated across batches using reciprocal principal component analysis (RPCAIntegration). A principal component analysis and uniform manifold approximation and projection (UMAP) were performed, followed by the FindNeighbors and FindClusters functions. We opted to cluster at a low resolution (0.25) to differentiate aortic cell types and to identify only major subpopulations of smooth muscle cells that vary by a large number of differentially expressed genes. FindMarkers was used to identify cluster-defining transcripts and differentially expression genes between control and diseased cell populations based on a Wilcoxon rank sum test.

Reanalysis of human aortic cells from Pedroza et al. (2023). For reanalysis of the ascending aorta and aortic root samples from a recently published scRNA-seq dataset of the donors and aortas of patients with LDS³⁸, we used the following criteria: >1,000 transcripts detected per cell but <6,000 and >1,500 total molecules detected per cell <30,000 and <20% mitochondrial transcripts per cell. This reduces this dataset from 58,947 aortic cells to 43,349 for further analysis. We analyzed this dataset as described above with the FindClusters resolution parameter set to 0.15.

CoGAPS and projectR. CoGAPS³⁹ (v3.22), an R package that utilizes non-negative matrix factorization to uncover latent patterns of coordinated gene expression representative of shared biological functions, was used to identify transcriptional patterns associated with VSMC subpopulations, with the npatterns parameter set to 8, in scRNA-seq analysis of murine aortas. ProjectR⁴⁰ (v1.2), an R package that enables integration and analysis of multiple scRNA-seq datasets by identifying transcriptional patterns shared among datasets, was used to project these patterns into scRNA-seq analysis of the human aortic root and ascending aorta.

Gene over-representation analyses. ClueGO¹⁹ was used for gene over-representation analysis and visualization of enriched functional terms for transcripts globally dysregulated in all VSMCs as well as VSMC subsets.

The transcripts were filtered on the basis of an adjusted *P* value less than 0.05 and an average absolute log₂ fold change of 0.25 or greater, as well as detection in at least 20% of either the control or LDS VSMCs. The resulting list of 502 downregulated and 200 upregulated genes was compared against five gene ontology databases (MSigDB Hallmark, KEGG, WikiPathways, Bioplane and Reactome). The list of transcripts and ClueGO log files are provided in Supplementary Tables 2, 7 and 8. Differentially expressed gene lists were also analyzed using the online gene list enrichment analysis tool EnrichR^{25,41,42} (<https://maayanlab.cloud/Enrichr/>) for pathways using MSigDB^{43,44} and for transcription factors target enrichment using the ENCODE²³ and ChEA²⁴ databases.

MERFISH spatial transcriptomics. MERFISH spatial transcriptomics using a custom panel was performed on 5 μm formalin-fixed paraffin-embedded sections of control and LDS aortas according to manufacturer's protocols (MERSCOPE Formalin-Fixed Paraffin-Embedded Tissue Sample Preparation User Guide Rev B, Vizgen). The slides were processed and imaged on a MERSCOPE instrument platform according to the manufacturer's protocols (MERSCOPE Instrument User Guide Rev G, Vizgen). The raw images were processed by the instrument software to generate a matrix of spatial genomics measurements and associated image files that were analyzed using the MERSCOPE visualizer software.

Statistics

GraphPad Prism 10.0 was used for data visualization and statistical analysis. The data were tested for normality using the Shapiro–Wilk test and upon verification of normal distribution were analyzed using a Brown–Forsythe analysis of variance (ANOVA) test. For echocardiographic and blood pressure measurements, the data are presented as a box and whisker plot with the whiskers indicating the maximum and minimum values and a horizontal bar indicating the median. All individual data points are shown as dots. The figures indicating statistical significance include the statistical tests used in the figure caption.

Reporting summary

Further information on research design is available in the Nature Portfolio Reporting Summary linked to this article.

Data availability

All scRNA-seq data, both raw fastq files and aggregated matrixes, is available in the Gene Expression Omnibus repository under accession number [GSE267204](https://www.ncbi.nlm.nih.gov/geo/query/acc.cgi?acc=GSE267204). MERFISH data are available on Dataverse via <https://dataverse.harvard.edu/dataverse/Gata4LDSAorticDilation> (ref. 65).

Code availability

R Scripts for scRNA-seq analysis using the Seurat, CoGAPS and ProjectR packages (as described in Methods) are available as a GitHub repository at <https://github.com/emilybramel/SingleCellRNAseqMurineAorta.git>.

References

1. Chou, E., Pirruccello, J. P., Ellinor, P. T. & Lindsay, M. E. Genetics and mechanisms of thoracic aortic disease. *Nat. Rev. Cardiol.* **20**, 168–180 (2023).
2. MacCarrick, G. et al. Loeys–Dietz syndrome: a primer for diagnosis and management. *Genet. Med.* **16**, 576–587 (2014).
3. Loeys, B. L. et al. A syndrome of altered cardiovascular, craniofacial, neurocognitive and skeletal development caused by mutations in TGFBR1 or TGFBR2. *Nat. Genet.* **37**, 275–281 (2005).
4. van de Laar, I. M. et al. Mutations in SMAD3 cause a syndromic form of aortic aneurysms and dissections with early-onset osteoarthritis. *Nat. Genet.* **43**, 121–126 (2011).
5. Lindsay, M. E. et al. Loss-of-function mutations in TGFB2 cause a syndromic presentation of thoracic aortic aneurysm. *Nat. Genet.* **44**, 922–927 (2012).
6. Bertoli-Avella, A. M. et al. Mutations in a TGF-beta ligand, TGFB3, cause syndromic aortic aneurysms and dissections. *J. Am. Coll. Cardiol.* **65**, 1324–1336 (2015).
7. Micha, D. et al. SMAD2 mutations are associated with arterial aneurysms and dissections. *Hum. Mutat.* **36**, 1145–1149 (2015).
8. van de Laar, I. M. et al. Phenotypic spectrum of the SMAD3-related aneurysms-osteoarthritis syndrome. *J. Med. Genet.* **49**, 47–57 (2012).
9. Gallo, E. M. et al. Angiotensin II-dependent TGF-β signaling contributes to Loeys–Dietz syndrome vascular pathogenesis. *J. Clin. Invest.* **124**, 448–460 (2014).

10. MacFarlane, E. G. et al. Lineage-specific events underlie aortic root aneurysm pathogenesis in Loeys–Dietz syndrome. *J. Clin. Invest.* **129**, 659–675 (2019).
11. Williams, J. A. et al. Early surgical experience with Loeys–Dietz: a new syndrome of aggressive thoracic aortic aneurysm disease. *Ann. Thorac. Surg.* **83**, S757–S763 (2007).
12. Hughes, G. C. Aggressive aortic replacement for Loeys–Dietz syndrome. *Tex. Heart Inst. J.* **38**, 663–666 (2011).
13. Patel, N. D. et al. Aortic root replacement for children with Loeys–Dietz Syndrome. *Ann. Thorac. Surg.* **103**, 1513–1518 (2017).
14. Bersi, M. R., Bellini, C., Humphrey, J. D. & Avril, S. Local variations in material and structural properties characterize murine thoracic aortic aneurysm mechanics. *Biomech. Model. Mechanobiol.* **18**, 203–218 (2019).
15. Gong, J. et al. In vitro lineage-specific differentiation of vascular smooth muscle cells in response to SMAD3 deficiency: implications for SMAD3-related thoracic aortic aneurysms. *Arterioscler. Thromb. Vasc. Biol.* **40**, 1651–1663 (2020).
16. Kalluri, A. S. et al. Single-cell analysis of the normal mouse aorta reveals functionally distinct endothelial cell populations. *Circulation* **140**, 147–163 (2019).
17. Michel, J. B., Jondeau, G. & Milewicz, D. M. From genetics to response to injury: vascular smooth muscle cells in aneurysms and dissections of the ascending aorta. *Cardiovasc. Res.* **114**, 578–589 (2018).
18. Shannon, P. et al. Cytoscape: a software environment for integrated models of biomolecular interaction networks. *Genome Res.* **13**, 2498–2504 (2003).
19. Bindea, G. et al. ClueGO: a Cytoscape plug-in to decipher functionally grouped gene ontology and pathway annotation networks. *Bioinformatics* **25**, 1091–1093 (2009).
20. Yamashiro, Y. et al. Role of thrombospondin-1 in mechanotransduction and development of thoracic aortic aneurysm in mouse and humans. *Circ. Res.* **123**, 660–672 (2018).
21. Bunton, T. E. et al. Phenotypic alteration of vascular smooth muscle cells precedes elastolysis in a mouse model of Marfan syndrome. *Circ. Res.* **88**, 37–43 (2001).
22. Bramel, E. E. et al. Postnatal Smad3 inactivation in murine smooth muscle cells elicits a temporally and regionally distinct transcriptional response. *Front. Cardiovasc. Med.* **9**, 826495 (2022).
23. Luo, Y. et al. New developments on the Encyclopedia of DNA Elements (ENCODE) data portal. *Nucleic Acids Res.* **48**, D882–D889 (2020).
24. Lachmann, A. et al. ChEA: transcription factor regulation inferred from integrating genome-wide ChIP-X experiments. *Bioinformatics* **26**, 2438–2444 (2010).
25. Xie, Z. et al. Gene set knowledge discovery with enrichr. *Curr. Protoc.* **1**, e90 (2021).
26. Ashino, T., Yamamoto, M., Yoshida, T. & Numazawa, S. Redox-sensitive transcription factor Nrf2 regulates vascular smooth muscle cell migration and neointimal hyperplasia. *Arterioscler. Thromb. Vasc. Biol.* **33**, 760–768 (2013).
27. Chen, Y. H., Layne, M. D., Watanabe, M., Yet, S. F. & Perrella, M. A. Upstream stimulatory factors regulate preferentially expressed gene-1 expression in vascular smooth muscle cells. *J. Biol. Chem.* **276**, 47658–47663 (2001).
28. Sellak, H., Choi, C., Browner, N. & Lincoln, T. M. Upstream stimulatory factors (USF-1/USF-2) regulate human cGMP-dependent protein kinase I gene expression in vascular smooth muscle cells. *J. Biol. Chem.* **280**, 18425–18433 (2005).
29. Wang, Q. et al. A hierarchical and collaborative BRD4/CEBPB partnership governs vascular smooth muscle cell inflammation. *Mol. Ther. Methods Clin. Dev.* **21**, 54–66 (2021).
30. Ko, C. Y., Chang, W. C. & Wang, J. M. Biological roles of CCAAT/enhancer-binding protein delta during inflammation. *J. Biomed. Sci.* **22**, 6 (2015).
31. Herzig, T. C. et al. Angiotensin II type1a receptor gene expression in the heart: AP-1 and GATA-4 participate in the response to pressure overload. *Proc. Natl Acad. Sci. USA* **94**, 7543–7548 (1997).
32. Bramel, E. E. et al. Distinct contribution of global and regional angiotensin II type 1a receptor inactivation to amelioration of aortopathy in *Tgfb1*^{M318R/+} mice. *Front. Cardiovasc. Med.* **9**, 936142 (2022).
33. Ren, Q. et al. C/EBPβ: the structure, regulation, and its roles in inflammation-related diseases. *Biomed. Pharmacother.* **169**, 115938 (2023).
34. Mondal, T. et al. MEG3 long noncoding RNA regulates the TGF-β pathway genes through formation of RNA–DNA triplex structures. *Nat. Commun.* **6**, 7743 (2015).
35. Liu, S. et al. LncRNA CARMN inhibits abdominal aortic aneurysm formation and vascular smooth muscle cell phenotypic transformation by interacting with SRF. *Cell. Mol. Life Sci.* **81**, 175 (2024).
36. Zhou, D. et al. hiPSC modeling of lineage-specific smooth muscle cell defects caused by *TGFBR1*^{A230T} variant, and its therapeutic implications for Loeys–Dietz syndrome. *Circulation* **144**, 1145–1159 (2021).
37. Pedroza, A. J. et al. Embryologic origin influences smooth muscle cell phenotypic modulation signatures in murine marfan syndrome aortic aneurysm. *Arterioscler. Thromb. Vasc. Biol.* **42**, 1154–1168 (2022).
38. Pedroza, A. J. et al. Early clinical outcomes and molecular smooth muscle cell phenotyping using a prophylactic aortic arch replacement strategy in Loeys–Dietz syndrome. *J. Thorac. Cardiovasc. Surg.* **166**, e332–e376 (2023).
39. Johnson, J. A. I. et al. Inferring cellular and molecular processes in single-cell data with non-negative matrix factorization using Python, R and GenePattern Notebook implementations of CoGAPS. *Nat. Protoc.* **18**, 3690–3731 (2023).
40. Sharma, G., Colantuoni, C., Goff, L. A., Fertig, E. J. & Stein-O'Brien, G. projectR: an R/Bioconductor package for transfer learning via PCA, NMF, correlation and clustering. *Bioinformatics* **36**, 3592–3593 (2020).
41. Chen, E. Y. et al. Enrichr: interactive and collaborative HTML5 gene list enrichment analysis tool. *BMC Bioinf.* **14**, 128 (2013).
42. Kuleshov, M. V. et al. Enrichr: a comprehensive gene set enrichment analysis web server 2016 update. *Nucleic Acids Res.* **44**, W90–W97 (2016).
43. Liberzon, A. et al. The Molecular Signatures Database (MSigDB) hallmark gene set collection. *Cell Syst.* **1**, 417–425 (2015).
44. Castanza, A. S. et al. Extending support for mouse data in the Molecular Signatures Database (MSigDB). *Nat. Methods* **20**, 1619–1620 (2023).
45. Korbecki, J., Maruszewska, A., Bosiacki, M., Chlubek, D. & Baranowska-Bosiacka, I. The potential importance of CXCL1 in the physiological state and in noncancer diseases of the cardiovascular system, respiratory system and skin. *Int. J. Mol. Sci.* <https://doi.org/10.3390/ijms24010205> (2022).
46. Shen, Y. et al. IRF-1 contributes to the pathological phenotype of VSMCs during atherogenesis by increasing CCL19 transcription. *Aging* **13**, 933–943 (2020).
47. Kang, C. et al. The DNA damage response induces inflammation and senescence by inhibiting autophagy of GATA4. *Science* **349**, aaa5612 (2015).
48. Yap, C., Mieremet, A., de Vries, C. J. M., Micha, D. & de Waard, V. Six shades of vascular smooth muscle cells illuminated by KLF4 (Krueppel-like factor 4). *Arterioscler. Thromb. Vasc. Biol.* **41**, 2693–2707 (2021).

49. Jeong, K. et al. Nuclear focal adhesion kinase controls vascular smooth muscle cell proliferation and neointimal hyperplasia through GATA4-mediated cyclin D1 transcription. *Circ. Res.* **125**, 152–166 (2019).
50. Watt, A. J., Battle, M. A., Li, J. & Duncan, S. A. GATA4 is essential for formation of the proepicardium and regulates cardiogenesis. *Proc. Natl Acad. Sci. USA* **101**, 12573–12578 (2004).
51. Wirth, A. et al. G12-G13-LARG-mediated signaling in vascular smooth muscle is required for salt-induced hypertension. *Nat. Med.* **14**, 64–68 (2008).
52. Wagenseil, J. E. & Mecham, R. P. Vascular extracellular matrix and arterial mechanics. *Physiol. Rev.* **89**, 957–989 (2009).
53. van Dorst, D. C. H. et al. Transforming growth factor- β and the renin–angiotensin system in syndromic thoracic aortic aneurysms: implications for treatment. *Cardiovasc. Drugs Ther.* <https://doi.org/10.1007/s10557-020-07116-4> (2020).
54. Daugherty, A., Sawada, H., Sheppard, M. B. & Lu, H. S. Angiotensinogen as a therapeutic target for cardiovascular and metabolic diseases. *Arterioscler. Thromb. Vasc. Biol.* **44**, 1021–1030 (2024).
55. Pedroza, A. J. et al. Single-cell transcriptomic profiling of vascular smooth muscle cell phenotype modulation in Marfan syndrome aortic aneurysm. *Arterioscler. Thromb. Vasc. Biol.* <https://doi.org/10.1161/ATVBAHA.120.314670> (2020).
56. Clement, M. et al. Vascular smooth muscle cell plasticity and autophagy in dissecting aortic aneurysms. *Arterioscler. Thromb. Vasc. Biol.* **39**, 1149–1159 (2019).
57. Pikkarainen, S. et al. GATA-4 is a nuclear mediator of mechanical stretch-activated hypertrophic program. *J. Biol. Chem.* **278**, 23807–23816 (2003).
58. Lino Cardenas, C. L. et al. An HDAC9-MALAT1-BRG1 complex mediates smooth muscle dysfunction in thoracic aortic aneurysm. *Nat. Commun.* **9**, 1009 (2018).
59. Wang, Y. Q., Batool, A., Chen, S. R. & Liu, Y. X. GATA4 is a negative regulator of contractility in mouse testicular peritubular myoid cells. *Reproduction* **156**, 343–351 (2018).
60. Smith, J. D., Chen, J. Z., Phillips, R., Daugherty, A. & Sheppard, M. B. Losartan Increases Survival of the *Fbn1*^{mgR/mgR} mouse model of Marfan syndrome in an age-dependent manner. Preprint at *bioRxiv* <https://doi.org/10.1101/2021.02.19.429438> (2021).
61. Yang, B. et al. Protein-altering and regulatory genetic variants near GATA4 implicated in bicuspid aortic valve. *Nat. Commun.* **8**, 15481 (2017).
62. Garg, V. et al. GATA4 mutations cause human congenital heart defects and reveal an interaction with TBX5. *Nature* **424**, 443–447 (2003).
63. Lepage, D. et al. Gata4 is critical to maintain gut barrier function and mucosal integrity following epithelial injury. *Sci. Rep.* **6**, 36776 (2016).
64. Zhou, P., He, A. & Pu, W. T. Regulation of GATA4 transcriptional activity in cardiovascular development and disease. *Curr. Top. Dev. Biol.* **100**, 143–169 (2012).
65. Bramel, E. E. MERFISH data for thoracic aorta of control and Loews–Dietz syndrome mice. V1. *Harvard Dataverse* <https://doi.org/10.7910/DVN/KZWIFX> (2024).

Acknowledgements

Research in this publication was supported by the National Heart, Lung, and Blood Institute of the National Institutes of Health under award numbers R01HL147947 to E.G.M. and F31HL163924 to E.E.B., as well as a generous gift from the Loews–Dietz Foundation. Fluorescence Microscopy imaging was also supported by NIH award number S10OD023548 to the School of Medicine Microscope Facility.

Author contributions

E.G.M. and E.E.B. conceptualized the study, designed the experiments, interpreted data, and prepared the manuscript. E.E.B. and T.J.C. generated and processed the scRNA-seq sequencing data. E.E.B. conducted the primary analysis of the scRNA-seq data and performed a reanalysis of published scRNA-seq datasets, with input from W.A.E.C., T.J.C., L.R. and J.T.M. E.G.M. conducted gene over-representation analysis and visualization. E.E.B., E.G.M., W.A.E. and L.R. were involved in sample preparation and processing for MERFISH. E.E.B. conducted in situ hybridization, immunofluorescence and immunoblotting experiments. E.E.B. was responsible for echocardiography, blood pressure measurements, genotyping and animal husbandry with support from T.J.C., M.S., W.A.E.C., L.R. and R.B. A.Z. performed histological staining and imaging. G.L.S.O. provided support for CoGAPS analysis and MERFISH high throughput in situ hybridization. A.J.P. and M.P.F. provided human scRNA-seq data and offered valuable insight on interpretation of the analysis. H.C.D. provided valuable input on the study design. E.G.M. and E.E.B. wrote the manuscript, and all authors contributed to its revision.

Competing interests

The authors declare no competing interests.

Additional information

Extended data is available for this paper at <https://doi.org/10.1038/s44161-024-00562-5>.

Supplementary information The online version contains supplementary material available at <https://doi.org/10.1038/s44161-024-00562-5>.

Correspondence and requests for materials should be addressed to Elena Gallo MacFarlane.

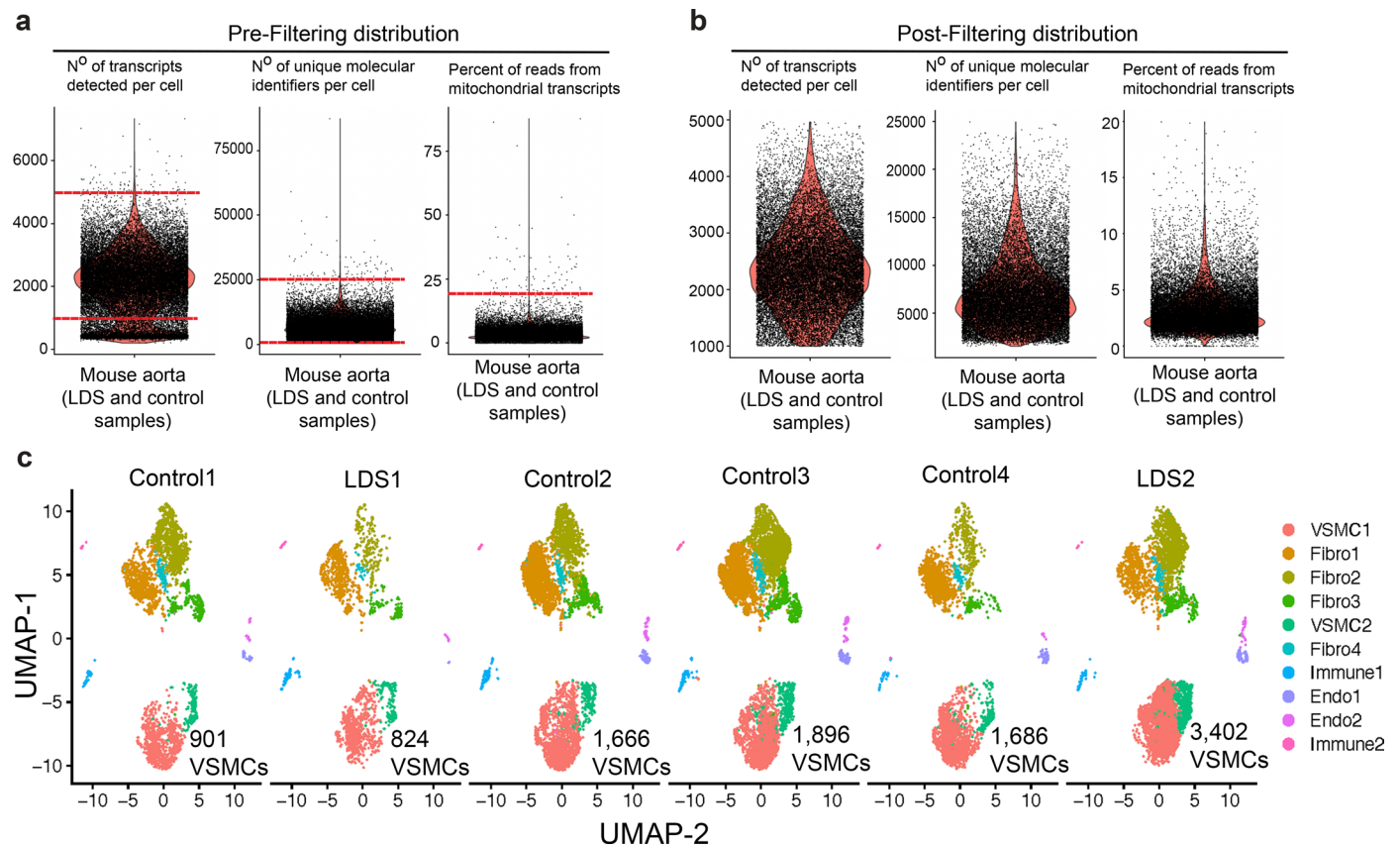
Peer review information *Nature Cardiovascular Research* thanks Helle Jorgensen, and the other, anonymous, reviewer(s) for their contribution to the peer review of this work.

Reprints and permissions information is available at www.nature.com/reprints.

Publisher's note Springer Nature remains neutral with regard to jurisdictional claims in published maps and institutional affiliations.

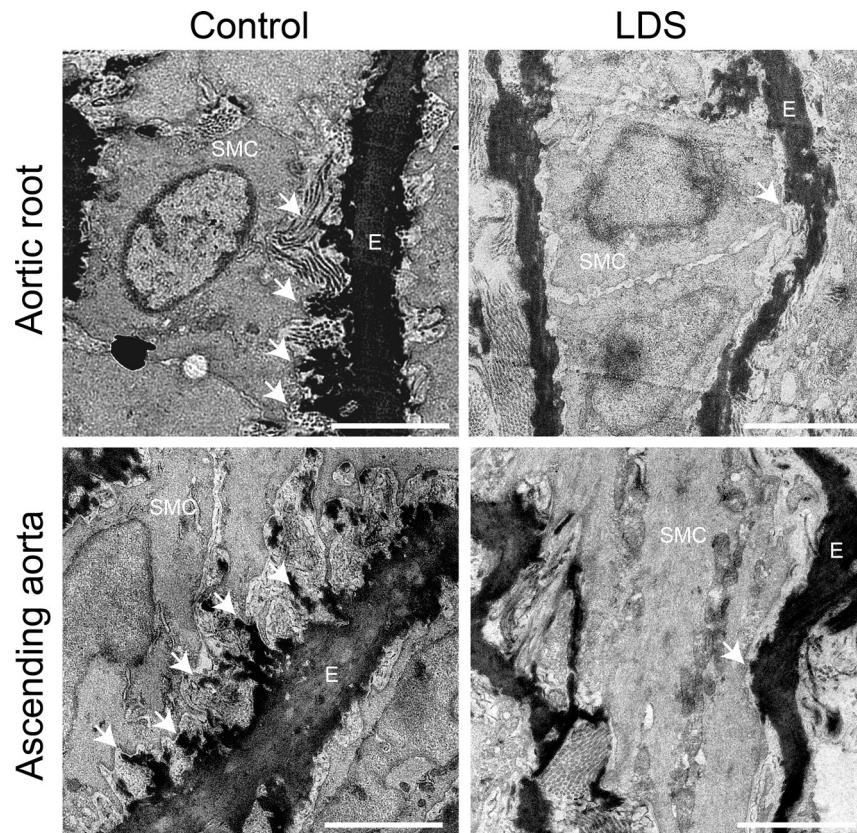
Open Access This article is licensed under a Creative Commons Attribution-NonCommercial-NoDerivatives 4.0 International License, which permits any non-commercial use, sharing, distribution and reproduction in any medium or format, as long as you give appropriate credit to the original author(s) and the source, provide a link to the Creative Commons licence, and indicate if you modified the licensed material. You do not have permission under this licence to share adapted material derived from this article or parts of it. The images or other third party material in this article are included in the article's Creative Commons licence, unless indicated otherwise in a credit line to the material. If material is not included in the article's Creative Commons licence and your intended use is not permitted by statutory regulation or exceeds the permitted use, you will need to obtain permission directly from the copyright holder. To view a copy of this licence, visit <http://creativecommons.org/licenses/by-nc-nd/4.0/>.

© The Author(s) 2024



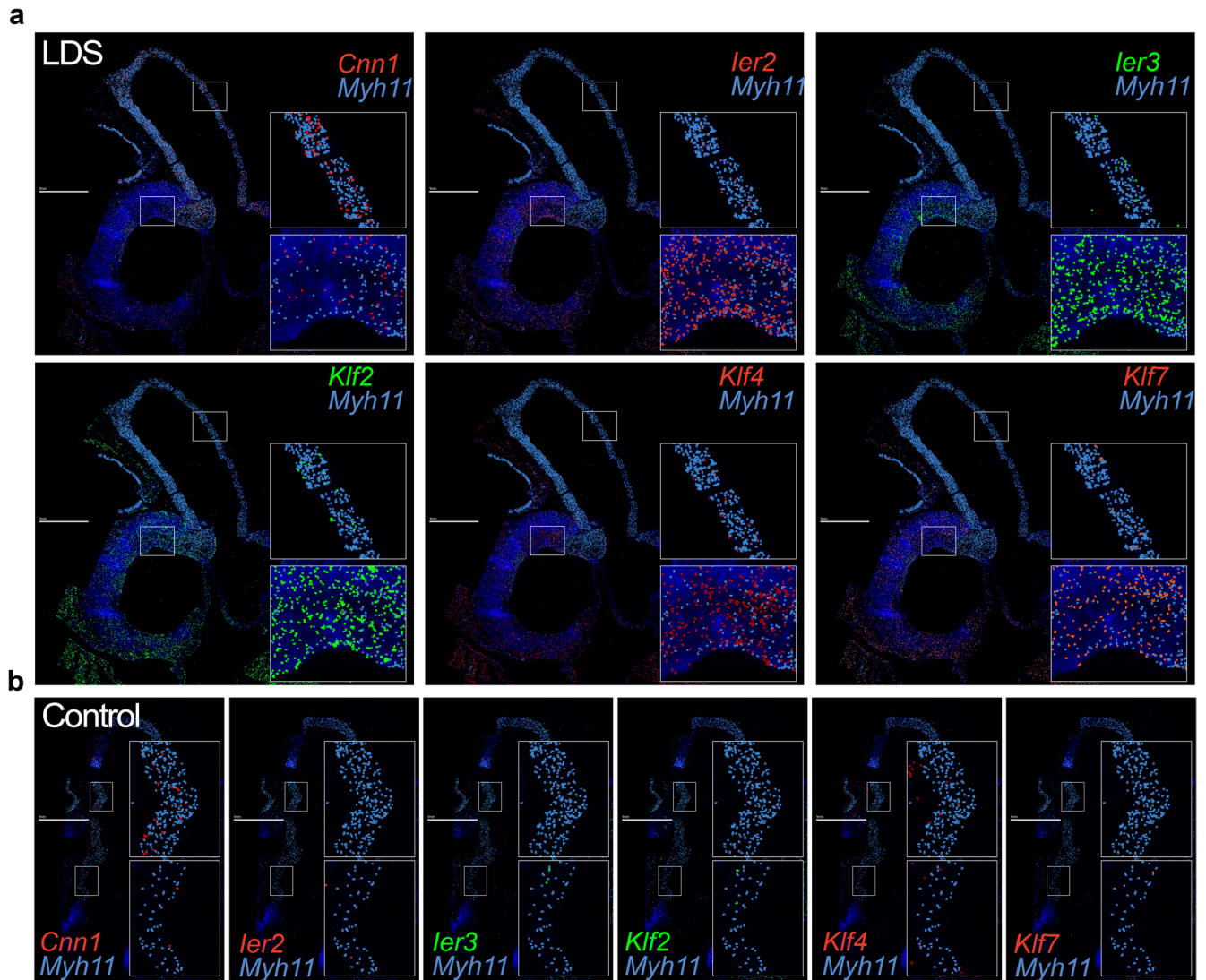
Extended Data Fig. 1 | Quality control and filtering of scRNAseq of murine aorta. ScRNAseq datasets from female control and *Tgfb1*^{M318R/+} LDS mice were filtered by the number of transcripts per cell (nFeature), number of unique molecular identifiers per cell (nCounts), and the percent of reads from mitochondrial transcripts. Density plots showing the distribution of aortic cells from control and *Tgfb1*^{M318R/+} LDS mice pre-filtering (**a**) and post-filtering (**b**) based on the following cutoffs which are indicated in the figure by horizontal

bars: >1000 nFeature <5000, >1500 nCounts <25000, and <20% mitochondrial transcripts per cell. (**c**) UMAP of murine scRNAseq data split by mouse ID, showing the distribution of cells from each independent biological replicate (n = 6, 2 LDS and 4 control). Samples are labeled by genotype and the number of VSMCs per sample is indicated. A total of 4,226 LDS VSMCs and 6,149 control VSMCs were included in subsequent analyses.



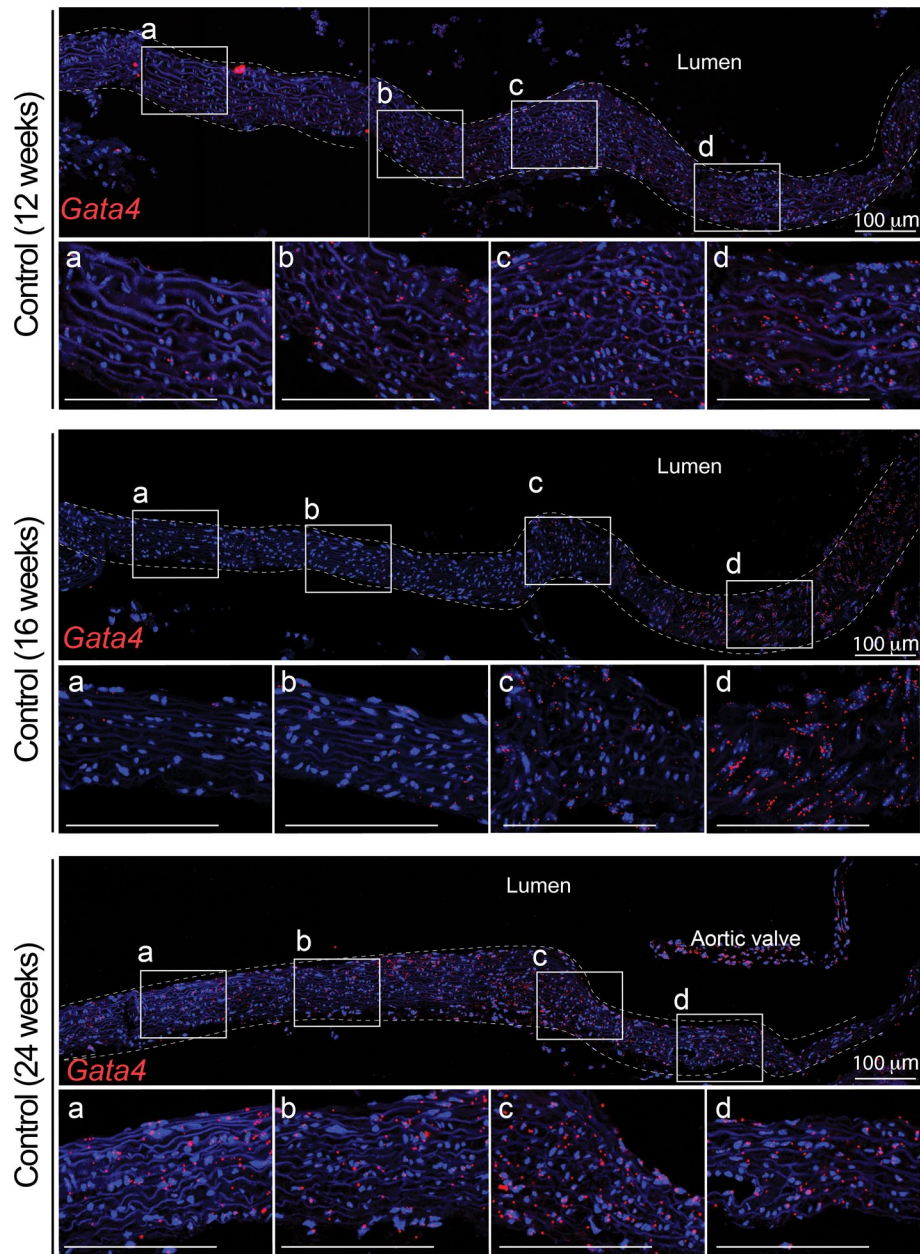
Extended Data Fig. 2 | Defective connections between smooth muscle cells and elastic lamellae in the aorta of LDS mice. Electron micrographs of longitudinal sections of the aortic root and ascending aorta of control and LDS mice at 6 weeks of age. Elastic fibers are stained dark (E, elastic lamellae;

SMC, smooth muscle cell). Arrows indicate examples of dense plaques, which mark connections between elastic lamellae and smooth muscle cells. Image representative of three independent biological replicates. Scale bar is 2 microns.



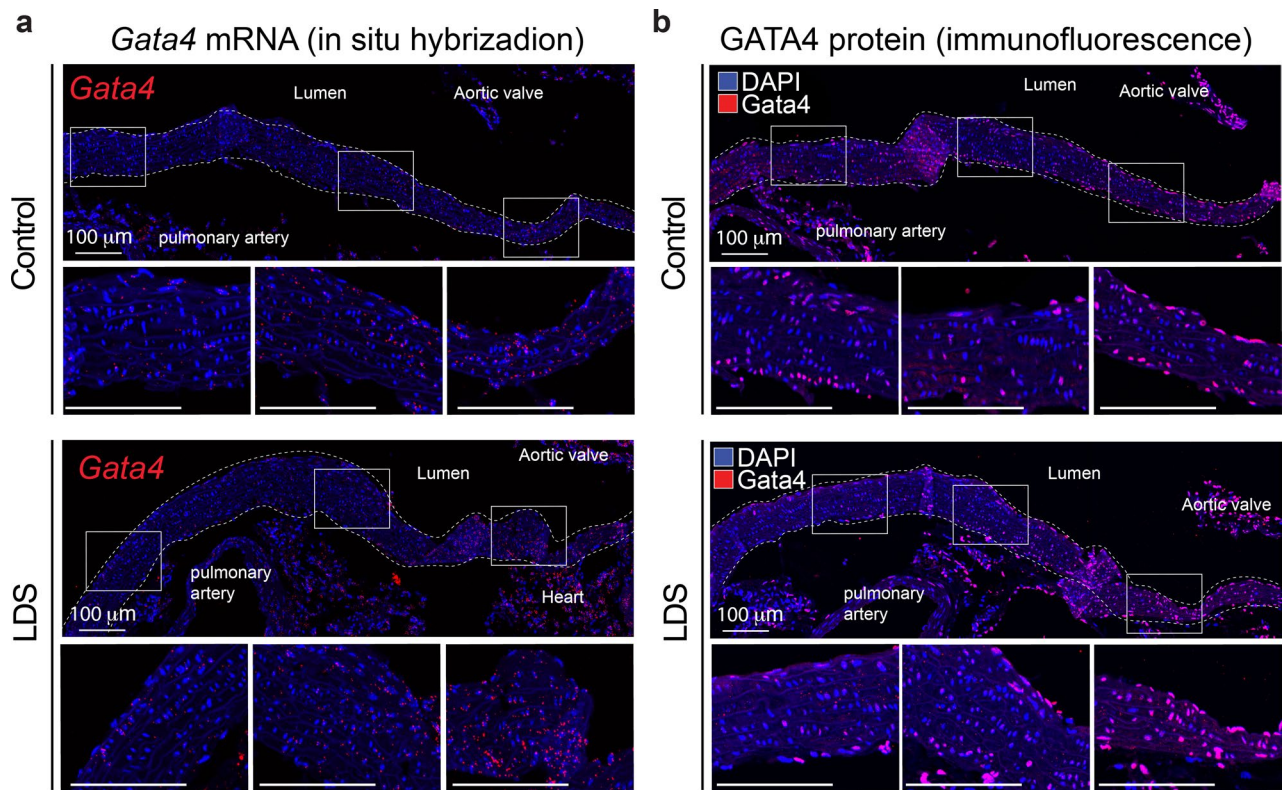
Extended Data Fig. 3 | MERFISH reveals spatially heterogeneous expression of transcripts coding for Calponin-1, Immediate Early Response genes, and Kruppel-like Factor genes in LDS VSMCs. MERFISH images of the proximal aorta of male LDS (a) and male control (b) mice at 16 weeks of age, scale bar is 1 mm. Experiment was conducted once on one pair of age and sex-matched

samples. Scale bar is 1 mm. Panels depict the colocalization of *Myh11* and transcripts of interest in the aorta of LDS (a) and control (b) mice. Insets denote regions of the ascending aorta and aortic root that are presented at higher magnification.



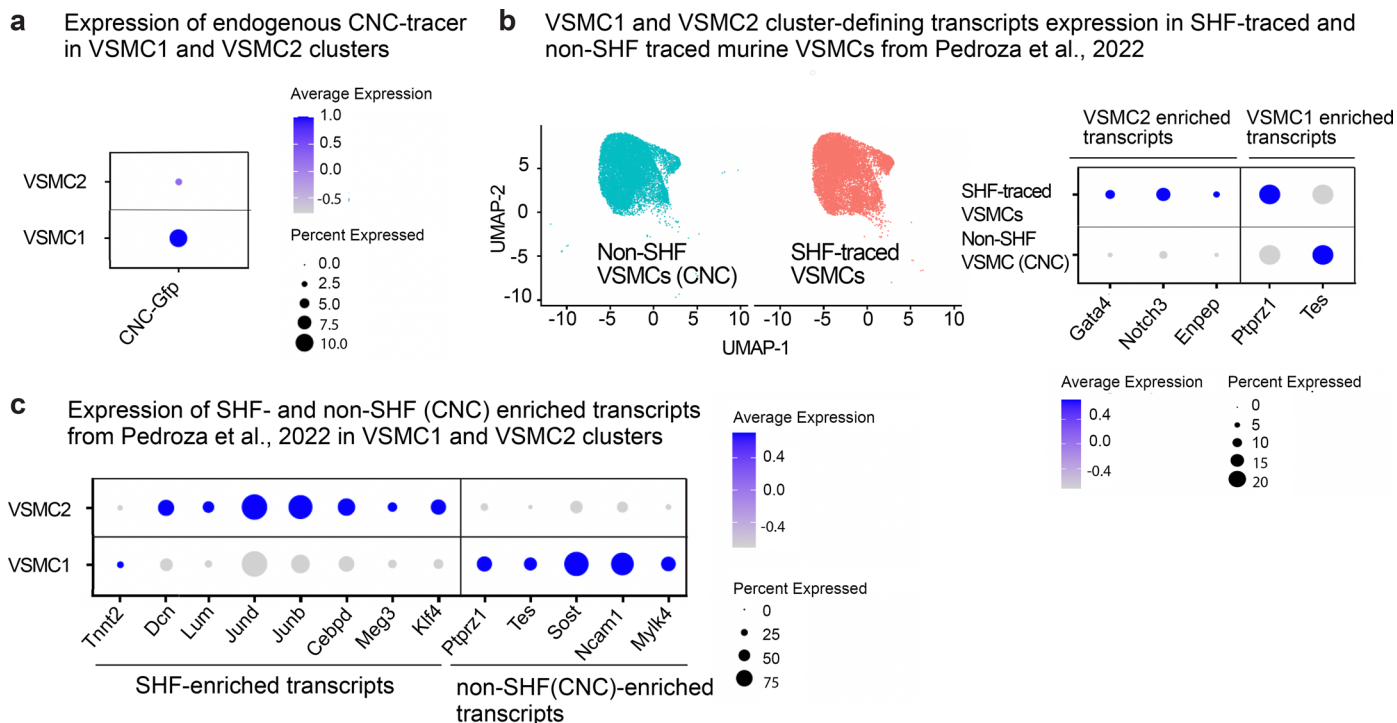
Extended Data Fig. 4 | Expression of *Gata4* transcript correlates with location along the proximal-to-distal axis in the mouse aorta. RNA in situ hybridization showing the expression of *Gata4* along the length of the murine aorta in 12-, 16- and 24-week-old control animals (three independent biological samples

are shown; representative of two experiments showing similar results). Insets identify the location shown at higher magnification in the subsequent panel. The dashed line identifies the approximate boundaries of the aortic wall. Scale bar is 100 microns.



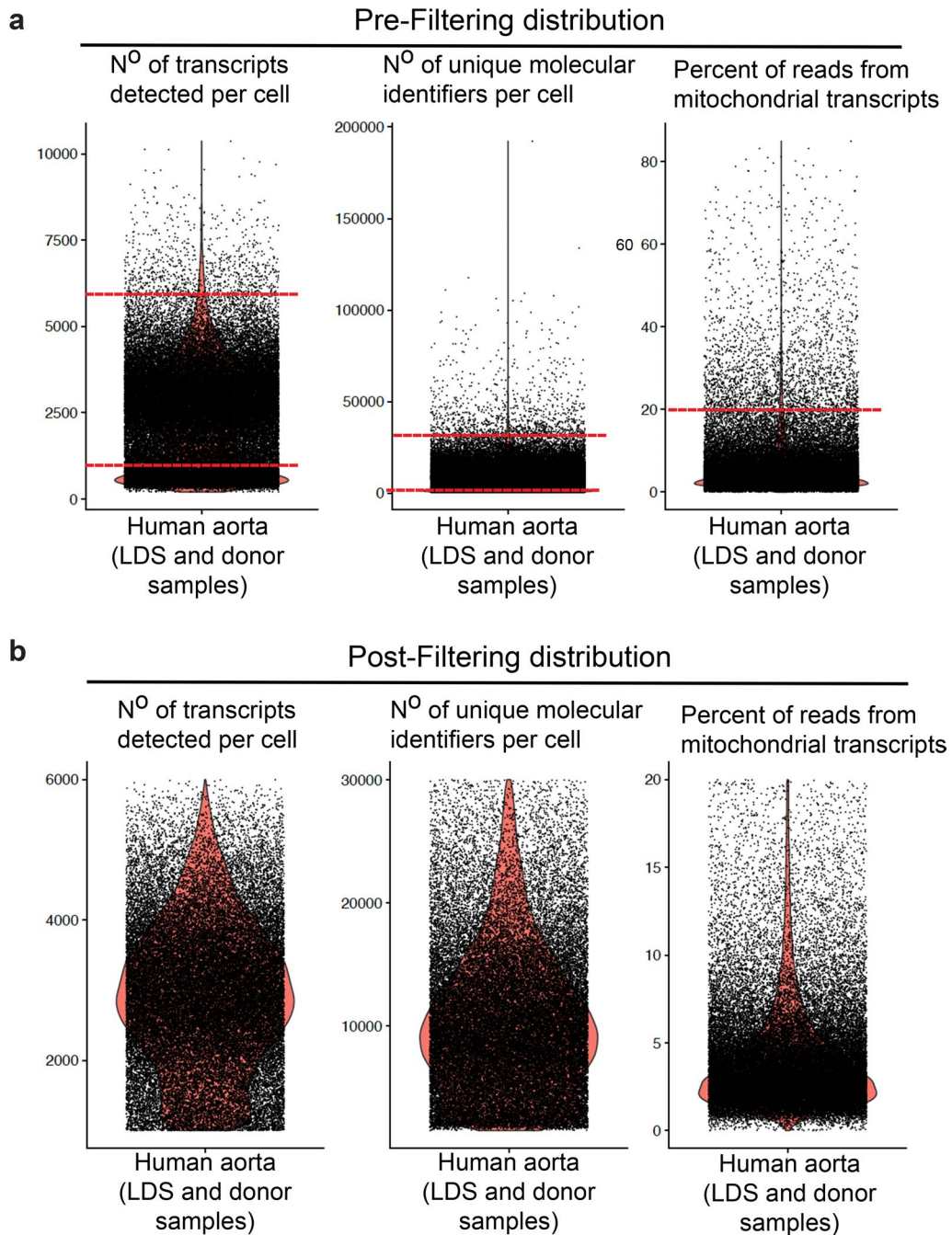
Extended Data Fig. 5 | *Gata4* mRNA and protein are upregulated in the aortic root of LDS mice. (a) RNA in situ hybridization for *Gata4* in the aortic root and ascending aorta of male control and LDS (*Tgfbr1*^{M318R/+}) mice, representative of 5 independent biological replicates. Insets identify the location shown at higher magnification in the subsequent panel. Scale bar is 100 microns.

(b) Immunofluorescence for Gata4 in the aortic root and ascending aorta of male control and LDS mice. Insets identify the location shown at higher magnification in the subsequent panel, representative of 4 independent biological replicates. Scale bar is 100 microns. The dashed line identifies the approximate boundaries of the aortic wall.



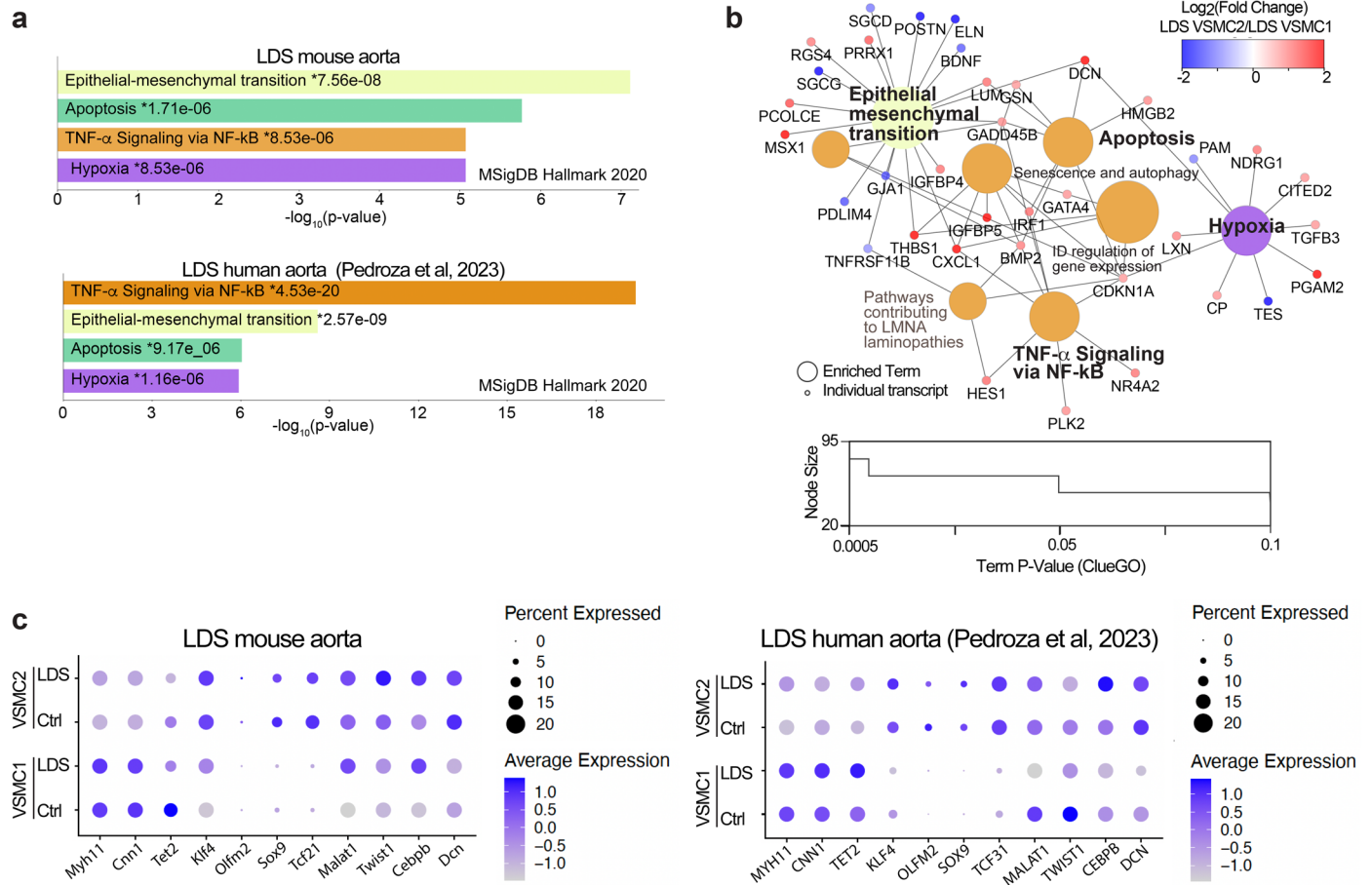
Extended Data Fig. 6 | VSMC1 and VSMC2 subclusters correlate but do not overlap with lineage-of-origin. (a) A subset of cells included in the analysis derived from mice carrying the Rosa26-flox-STOP-flox-EGFP-L10a transgene and a Cre recombinase expressed under the control of a CNC-specific Wnt2 promoter (Wnt2-Cre). Dot plot shows detection of the *Gfp* reporter in VSMC1 and VSMC2. The color of the dot represents a scaled average expression while the size

indicates the percentage of cells in which *Gfp* was detected. (b) UMAP of SHF-traced and non-SHF traced VSMCs and dot plot showing the SHF and non-SHF, and therefore CNC, enriched transcripts from Pedroza et al., 2022 in VSMC1 and VSMC2. (c) Dot plot of VSMC1 and VSMC2 cluster defining transcripts in SHF-traced and non-traced VSMCs from Pedroza et al., 2022.



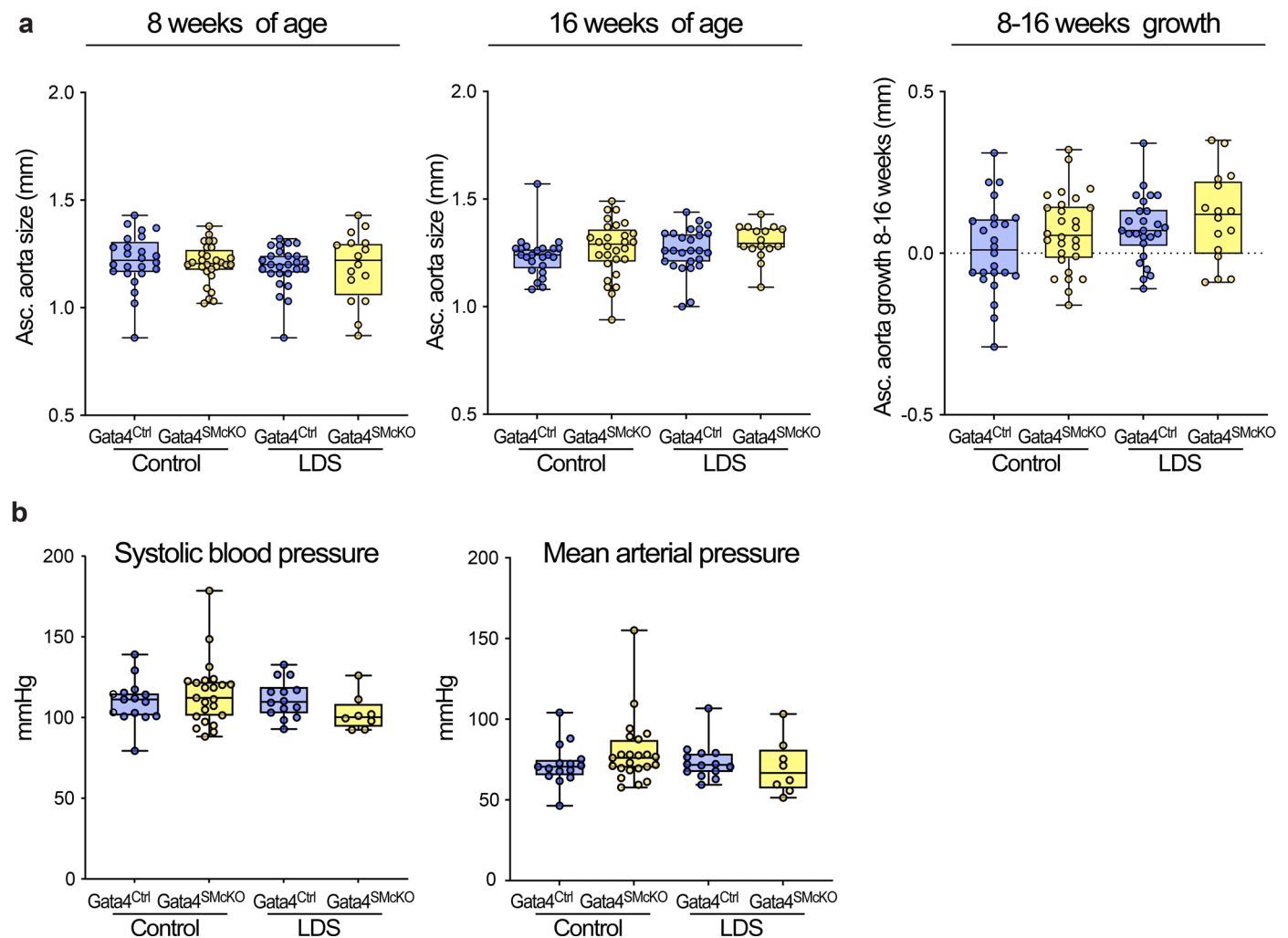
Extended Data Fig. 7 | Quality control and filtering of scRNAseq of human aorta. Published scRNAseq dataset of donor and LDS patient aortic cells (Pedroza et al., 2023) was re-analyzed and filtered by the number of transcripts per cell (nFeature), number of unique molecular identifiers per cell (nCounts), and the percent of reads from mitochondrial transcripts. Density plots show the

distribution of aortic cells from donor and LDS patients from pre-filtering (**a**) and post-filtering (**b**) based on the following cutoffs which are indicated in the figure by horizontal bars: >1000 nFeature < 6000 , > 30000 nCounts, and $< 20\%$ mitochondrial transcripts per cell.



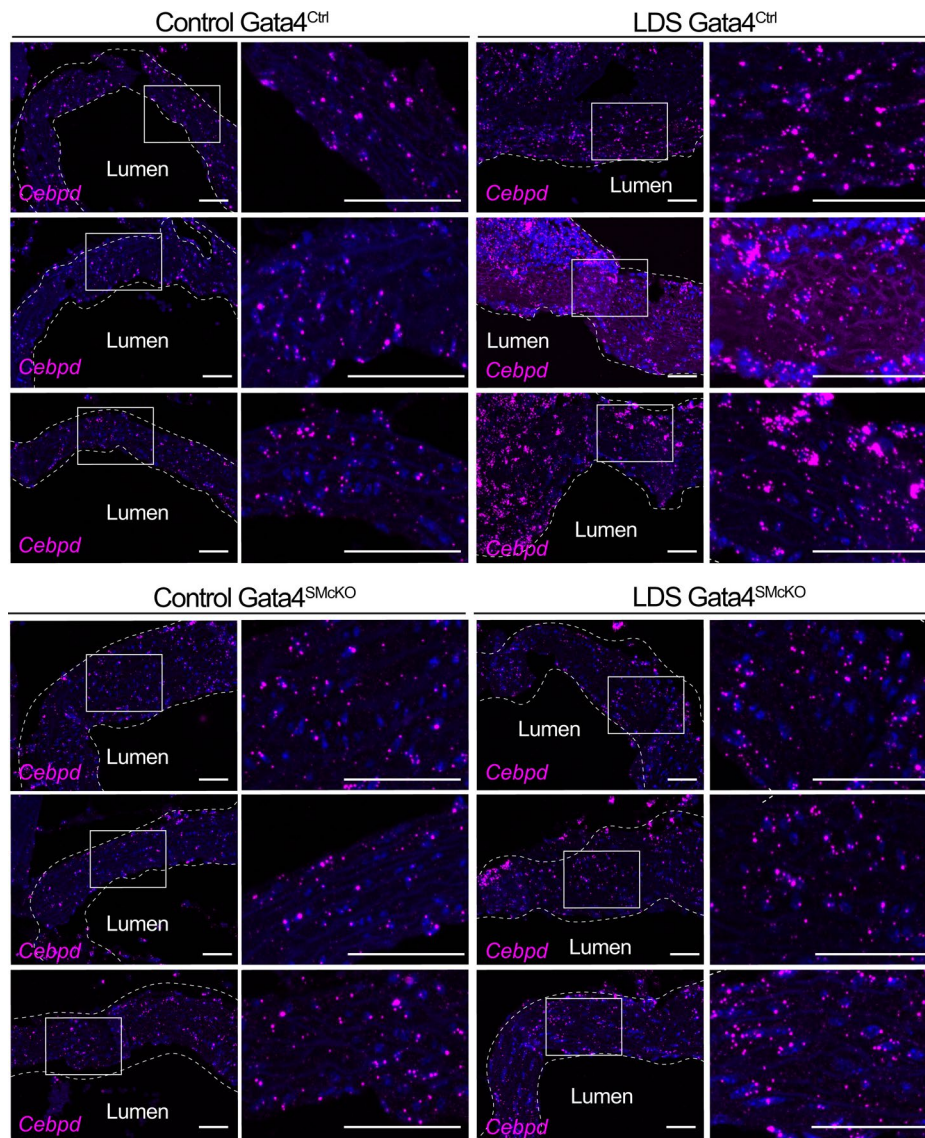
Extended Data Fig. 8 | VSMC2-defining transcripts are enriched in modulators of inflammation and cellular stress in both mouse and human aortas. (a) EnrichR bar plot of the top four significantly enriched pathways in the MSigDB Hallmark 2020 database in LDS VSMC2 relative to LDS VSMC1 in both mouse and human datasets. P-values refer to significance of enrichment. (b) Network visualization of MSigDB VSMC2-enriched pathways and biological terms with shared ClueGO grouping. The color of term nodes identifies ClueGO

biological grouping. Individual genes are colored by the Log_2 fold change of expression in LDS VSMC2 relative to LDS VSMC1 (blue genes are downregulated while red genes are upregulated in VSMC2 relative to VSMC1) (c) Dot plot of transcripts involved in modulation of VSMC contractile and non-contractile phenotypes in VSMC1 and VSMC2 in the mouse and human scRNAseq datasets. Color of the dot represents a scaled average expression, while the size indicates the percentage of cells in which the transcript was detected.



Extended Data Fig. 9 | Gata4 deletion does not affect size or growth of the ascending aorta or blood pressure in LDS mice. (a) Ascending aortic diameter of male Ctrl (*Tgfbri*^{+/+}) and LDS (*Tgfbri*^{M318R/+}) mice with (*Gata4*^{SMcko}) or without (*Gata4*^{Ctrl}) smooth muscle specific deletion of Gata4 as measured by echocardiography at 8 and 16 weeks of age, and aortic root growth from 8 to 16 weeks of age. The box plots show the upper quartile, median and lower quartile; each symbol represents an independent biological replicate; whiskers identify the minimum to maximum range (Ctrl *Gata4*^{Ctrl} n = 24; Ctrl *Gata4*^{SMcko} n = 28; LDS *Gata4*^{Ctrl} n = 26; LDS *Gata4*^{SMcko} n = 16). No significant differences were detected

(Brown-Forsythe ANOVA: 8 weeks $F^* = 0.31$, $DFn = 3$, $DFd = 52.88$, P value = 0.8142; 16 weeks $F^* = 1.39$, $DFn = 3$, $DFd = 87.78$, P value = 0.2491). (b) Systolic blood pressure and mean arterial pressure for male mice of the indicated genotypes. The box plots show the upper quartile, median and lower quartile; each symbol represents an independent biological replicate; whiskers identify the minimum to maximum range (Ctrl *Gata4*^{Ctrl} n = 15; Ctrl *Gata4*^{SMcko} n = 23; LDS *Gata4*^{Ctrl} n = 14; LDS *Gata4*^{SMcko} n = 8). No significant differences were detected (Brown-Forsythe ANOVA: Systolic pressure $F^* = 1.465$, $DFn = 3$, $DFd = 53.86$, P value = 0.24; mean arterial $F^* = 1.055$, $DFn = 3$, $DFd = 38.74$, P value = 0.379).



Extended Data Fig. 10 | Smooth muscle-specific deletion of Gata4 results in reduced expression of *Cebpd*. RNA in situ hybridization for *Cebpd* in the aortic root of male mice of the indicated genotype at 16 weeks of age. Three independent biological replicates are shown per genotype, abbreviated as follows Control (*Tgfb1*^{+/+}) and LDS (*Tgfb1*^{M318R/+}) with (*Gata4*^{SMcKO}) or without

(*Gata4*^{Ctrl}) smooth muscle specific deletion of Gata4. Insets identify location shown at higher magnification in subsequent panels. Images were acquired at 20x magnification. Scale bars are 50 and 200 microns, respectively. The dashed line identifies the approximate boundaries of the aortic wall.

Reporting Summary

Nature Portfolio wishes to improve the reproducibility of the work that we publish. This form provides structure for consistency and transparency in reporting. For further information on Nature Portfolio policies, see our [Editorial Policies](#) and the [Editorial Policy Checklist](#).

Statistics

For all statistical analyses, confirm that the following items are present in the figure legend, table legend, main text, or Methods section.

- | n/a | Confirmed |
|-------------------------------------|---|
| <input type="checkbox"/> | <input checked="" type="checkbox"/> The exact sample size (n) for each experimental group/condition, given as a discrete number and unit of measurement |
| <input type="checkbox"/> | <input checked="" type="checkbox"/> A statement on whether measurements were taken from distinct samples or whether the same sample was measured repeatedly |
| <input type="checkbox"/> | <input checked="" type="checkbox"/> The statistical test(s) used AND whether they are one- or two-sided
<i>Only common tests should be described solely by name; describe more complex techniques in the Methods section.</i> |
| <input checked="" type="checkbox"/> | <input type="checkbox"/> A description of all covariates tested |
| <input type="checkbox"/> | <input checked="" type="checkbox"/> A description of any assumptions or corrections, such as tests of normality and adjustment for multiple comparisons |
| <input checked="" type="checkbox"/> | <input type="checkbox"/> A full description of the statistical parameters including central tendency (e.g. means) or other basic estimates (e.g. regression coefficient) AND variation (e.g. standard deviation) or associated estimates of uncertainty (e.g. confidence intervals) |
| <input type="checkbox"/> | <input checked="" type="checkbox"/> For null hypothesis testing, the test statistic (e.g. F , t , r) with confidence intervals, effect sizes, degrees of freedom and P value noted
<i>Give P values as exact values whenever suitable.</i> |
| <input checked="" type="checkbox"/> | <input type="checkbox"/> For Bayesian analysis, information on the choice of priors and Markov chain Monte Carlo settings |
| <input checked="" type="checkbox"/> | <input type="checkbox"/> For hierarchical and complex designs, identification of the appropriate level for tests and full reporting of outcomes |
| <input checked="" type="checkbox"/> | <input type="checkbox"/> Estimates of effect sizes (e.g. Cohen's d , Pearson's r), indicating how they were calculated |

Our web collection on [statistics for biologists](#) contains articles on many of the points above.

Software and code

Policy information about [availability of computer code](#)

Data collection

Data analysis

For manuscripts utilizing custom algorithms or software that are central to the research but not yet described in published literature, software must be made available to editors and reviewers. We strongly encourage code deposition in a community repository (e.g. GitHub). See the Nature Portfolio [guidelines for submitting code & software](#) for further information.

Data

Policy information about [availability of data](#)

All manuscripts must include a [data availability statement](#). This statement should provide the following information, where applicable:

- Accession codes, unique identifiers, or web links for publicly available datasets
- A description of any restrictions on data availability
- For clinical datasets or third party data, please ensure that the statement adheres to our [policy](#)

number GSE267204. MERFISH high throughput in situ hybridization data is available on Dataverse at <https://dataverse.harvard.edu/dataverse/Gata4LDSAorticDilation>.

Research involving human participants, their data, or biological material

Policy information about studies with [human participants or human data](#). See also policy information about [sex, gender \(identity/presentation\), and sexual orientation](#) and [race, ethnicity and racism](#).

Reporting on sex and gender	N/A
Reporting on race, ethnicity, or other socially relevant groupings	N/A
Population characteristics	N/A
Recruitment	N/A
Ethics oversight	N/A

Note that full information on the approval of the study protocol must also be provided in the manuscript.

Field-specific reporting

Please select the one below that is the best fit for your research. If you are not sure, read the appropriate sections before making your selection.

Life sciences Behavioural & social sciences Ecological, evolutionary & environmental sciences

For a reference copy of the document with all sections, see nature.com/documents/nr-reporting-summary-flat.pdf

Life sciences study design

All studies must disclose on these points even when the disclosure is negative.

Sample size	For smooth muscle specific deletion of Gata4 in Tgfb β 1M318R/+ mice (LDS) mice, sample size was predetermined by conducting a sample size power calculation (alpha 0.05, power 0.95) based on previously published aortic root diameters in LDS mice using the G*Power software (doi: 10.3352/jeehp.2021.18.17). This calculation determined that an n of 16 per group would be sufficient to determine statistically significant differences in aortic root growth.
Data exclusions	As there is some variability in the onset of aortic dilation in Tgfb β 1M318R/+ mice, and starting aortic size will affect final measurements, aortic root diameter of 1.9 mm and above at baseline (8 weeks of age) was defined a priori as an exclusion criterion.
Replication	Appropriate controls were used for every experiment including independent biological samples, and detailed methods have been provided to ensure reproducibility. Where relevant, experiments were replicated at least 3 times and all replications were successful. Details on the number of replications performed in addition to representative images shown are detailed in figure legends.
Randomization	Randomization is not relevant to this study, where groups are defined they are determined by the genotype of the mice.
Blinding	Echocardiographic images were read and measured by a researcher blinded to genotype. All other images (RNA in situ hybridization, histology, immunofluorescence) were also acquired by operator blinded to the genotype at the time of acquisition. Although the aortic phenotype of LDS mice is often immediately apparent, operators were blinded as to the state of the GATA4 locus, which is the relevant variable in this study.

Reporting for specific materials, systems and methods

We require information from authors about some types of materials, experimental systems and methods used in many studies. Here, indicate whether each material, system or method listed is relevant to your study. If you are not sure if a list item applies to your research, read the appropriate section before selecting a response.

Materials & experimental systems

n/a	<input type="checkbox"/>	<input checked="" type="checkbox"/> Involved in the study
	<input type="checkbox"/>	<input checked="" type="checkbox"/> Antibodies
	<input checked="" type="checkbox"/>	<input type="checkbox"/> Eukaryotic cell lines
	<input checked="" type="checkbox"/>	<input type="checkbox"/> Palaeontology and archaeology
	<input type="checkbox"/>	<input checked="" type="checkbox"/> Animals and other organisms
	<input checked="" type="checkbox"/>	<input type="checkbox"/> Clinical data
	<input checked="" type="checkbox"/>	<input type="checkbox"/> Dual use research of concern
	<input checked="" type="checkbox"/>	<input type="checkbox"/> Plants

Methods

n/a	<input type="checkbox"/>	<input checked="" type="checkbox"/> Involved in the study
	<input checked="" type="checkbox"/>	<input type="checkbox"/> ChIP-seq
	<input checked="" type="checkbox"/>	<input type="checkbox"/> Flow cytometry
	<input checked="" type="checkbox"/>	<input type="checkbox"/> MRI-based neuroimaging

Antibodies

Antibodies used	rabbit monoclonal antibody for GATA4 (D3A3M) (Cell Signaling Technology, CST36966) diluted 1:1000 for immunoblot and 1:100 for immunofluorescence mouse monoclonal antibody for β -Actin (8H10D10) (Cell Signaling Technology, CSTS3700) diluted 1:5000 for immunoblot donkey anti-rabbit secondary antibody Alexa Fluor 555 (ThermoFisher, A3279) diluted 1:10,000 for immunoblot
Validation	GATA4 CST36966: Validation statement provided by Cell Signaling Technology (accompanying image available online) Western blot analysis of extracts from various cell lines using GATA-4 (D3A3M) Rabbit mAb (upper) and GAPDH (D16H11) XP [®] Rabbit mAb #5174 (lower). As expected, HeLa cells exhibit very low GATA-4 expression. Reactivity: Monoclonal antibody is produced by immunizing animals with a synthetic peptide corresponding to residues near the amino terminus of human GATA-4 protein. Species predicted to react based on 100% sequence homology, mouse and rat. (https://www.cellsignal.com/products/primary-antibodies/gata-4-d3a3m-rabbit-mab/36966) β -Actin CST3700: Validation statement provided by Cell Signaling Technology (accompanying image available online) Western blot analysis of extracts from various cell types using β -Actin (8H10D10) Mouse mAb. Reactivity: Monoclonal antibody is produced by immunizing animals with a synthetic peptide corresponding to amino-terminal residues of human β -actin. β -Actin (8H10D10) Mouse mAb detects endogenous levels of total β -actin protein. Due to the high sequence identity between the cytoplasmic actin isoforms, β -actin and cytoplasmic γ -actin, this antibody may cross-react with cytoplasmic γ -actin. It does not cross-react with α -skeletal, α -cardiac, α -vascular smooth, or γ -enteric smooth muscle isoforms. Species: Human, Mouse, Rat, Hamster, Monkey, Dog. (https://www.cellsignal.com/products/primary-antibodies/b-actin-8h10d10-mouse-mab/3700)

Animals and other research organisms

Policy information about [studies involving animals](#); [ARRIVE guidelines](#) recommended for reporting animal research, and [Sex and Gender in Research](#)

Laboratory animals	Mice (<i>mus musculus</i>) were used for this study, strain and genotype information: <i>Tgfb1</i> ^{+/+} and <i>Tgfb1</i> ^{M318R/+} (The Jackson Laboratory, strain #036511) mice, some bearing the EGFP-L10a (The Jackson Laboratory, strain #024750) conditional tracer allele and a CNC-specific CRE recombinase expressed under the control of <i>Wnt2</i> promoter (The Jackson Laboratory, strain #003829) were used for scRNAseq as described in the Methods. All mice were maintained on a 129-background strain (Taconic, 129SVE). <i>Tgfb1</i> ^{+/+} and <i>Tgfb1</i> ^{M318R/+} mice were bred to <i>Gata4</i> ^{flox/flox} (The Jackson Laboratory, strain #008194) and mice carrying the <i>Myh11</i> -CreER transgene (The Jackson Laboratory, strain #019079). Mice were used for experiments at 16 weeks of age.
Wild animals	The study did not involve wild animals.
Reporting on sex	We have previously shown that there are no sex-specific differences in aortic dilation in the <i>Tgfb1</i> ^{M318R/+} LDS mouse model (doi:10.3389/fcvm.2022.936142), therefore we expect that all experiments performed regardless of the sex of the animals included will be relevant for both sexes. Aortas from female <i>Tgfb1</i> ^{+/+} and <i>Tgfb1</i> ^{M318R/+} mice were used for the scRNAseq dataset. For smooth muscle specific deletion of <i>Gata4</i> , a Cre integrated on the Y chromosome was used and therefore only male mice were used for this set of experiments.
Field-collected samples	This study did not involve samples collected from the field.
Ethics oversight	Animal experiments were conducted according to protocols approved by the Johns Hopkins University School of Medicine Animal Care and Use Committee (protocol number MO22M307).

Note that full information on the approval of the study protocol must also be provided in the manuscript.

Plants

Seed stocks

N/A

Novel plant genotypes

N/A

Authentication

N/A